

Determining the style and provenance of magmatic activity during the Early Aptian Oceanic Anoxic Event (OAE 1a)

L.M.E. Percival^{1*}; L.R. Tedeschi²; R.A. Creaser³; C. Bottini⁴; E. Erba⁴; F. Giraud⁵; H. Svensen⁶; J. Savian⁷; R. Trindade⁸; R. Coccioni⁹; F. Frontalini¹⁰; L. Jovane¹¹; T.A. Mather¹²; H.C. Jenkyns¹²

1: Analytical, Environmental and Geochemistry (AMGC) Group, Vrije Universiteit Brussel, Pleinlaan 2, 1050 Brussels, Belgium

2: Centro de Pesquisas e Desenvolvimento Leopoldo Américo Miguez de Mello (CENPES), Petróleo Brasileiro S.A., Avenida Horácio Macedo 950, 21941-915 Rio de Janeiro, Brazil

3: Department of Earth and Atmospheric Sciences, University of Alberta, Edmonton, Alberta, T6G 2E3, Canada

4: Dipartimento di Scienze della Terra, Università degli Studi di Milano, 20133 Milan, Italy

5: Université Grenoble Alpes, IRD, Université Savoie Mont Blanc, CNRS, Université Gustave Eiffel, ISTerre, 38000 Grenoble, France

6: The Center for Earth Evolution and Dynamics, University of Oslo, PO Box 1028 Blindern, 0315 Oslo, Norway

7: Departamento de Geologica, Universidade Federal do Rio Grande do Sul, 91501-970 Porto Alegre, Brazil

8: Departamento de Geofísica, Universidade de São Paulo, 05508-090 São Paulo, Brazil

9: Università degli Studi di Urbino “Carlo Bo”, 61029 Urbino, Italy

10: Dipartimento di Scienze Pure e Applicate, Università degli Studi di Urbino “Carlo Bo”, 61029 Urbino, Italy

11: Instituto Oceanográfico, Universidade de São Paulo, 05508-120 São Paulo, Brazil

12: Department of Earth Sciences, University of Oxford, South Parks Road, Oxford, OX1 3AN, UK

*Corresponding author: lawrence.percival@vub.be

KEYWORDS

Early Aptian Oceanic Anoxic Event (OAE 1a); mercury; osmium isotopes; Greater Ontong-Java Plateau; High Arctic Large Igneous Province; submarine LIP volcanism

30 **ABSTRACT**

31

32 Large igneous province (LIP) volcanism has been proposed as a key trigger of several
33 major climate and environmental perturbations during the Phanerozoic Aeon. Large-scale
34 carbon emissions associated with one or both of magmatic degassing from the Greater Ontong-
35 Java Plateau (G-OJP) and intrusion of organic-rich sediments by High Arctic LIP (HALIP) sills
36 have been widely suggested as the trigger of the Early Aptian Oceanic Anoxic Event (OAE 1a:
37 ~120 Ma). However, the respective roles of the two LIPs and associated carbon sources in causing
38 this crisis remain debated. Here, six records of OAE 1a from the Pacific, Tethyan, Arctic, and
39 South Atlantic realms are investigated, combining mercury (Hg) concentrations and osmium-
40 (Os-) isotope ratios as proxies of LIP activity. Together with previously published datasets, the
41 results indicate globally consistent Os-isotope evidence for LIP activity during OAE 1a, but
42 geographically variable stratigraphic Hg trends. Clear mercury enrichments that match Os-
43 isotope evidence of LIP activity, and suggest a Hg-cycle perturbation during the onset of OAE 1a,
44 are documented at one Pacific site extremely proximal to the G-OJP, but not in Arctic, Tethyan
45 or Atlantic records. This pattern highlights significant G-OJP volcanism during the onset of OAE
46 1a, and re-emphasises the limited potential for submarine LIP eruptions to cause Hg-cycle
47 perturbations except in areas very proximal to source. The absence of clear Hg peaks in basal
48 OAE 1a strata from the Arctic (or anywhere outside of the Pacific) does not support intense
49 HALIP activity at that time, suggesting that the G-OJP was the more volcanically active LIP
50 when OAE 1a commenced. Thus, G-OJP emissions of mantle carbon were more likely to have
51 played a major role in initiating OAE 1a than thermogenic volatiles associated with the HALIP.
52 A transient pulse of HALIP-related subaerial eruptions and/or thermogenic volatile emissions
53 during the early–middle part of OAE 1a, potentially evidenced by more widespread Hg
54 enrichments in strata from that time (including in the Arctic), might have prolonged the event.
55 However, a non-volcanic cause of these later Hg influxes cannot be excluded. These findings

challenge previous suggestions that magmatic CO₂ emissions from LIPs were incapable of causing major carbon-cycle perturbations alone, and highlight the need for further investigations to establish whether the high volume/emplacement rate of the G-OJP (potentially an order of magnitude greater than other LIPs) made it a unique case that stands in contrast to other provinces where the role of thermogenic volatiles was likely more crucial.

1. INTRODUCTION

Episodes of abrupt environmental perturbation occurred frequently throughout the Mesozoic Era, punctuating and/or superimposed upon longer term changes in climate (e.g., Jenkyns, 2010). The Early Aptian Oceanic Anoxic Event (OAE 1a, ~120 Ma) represented one of the most severe of these crises. Lasting ~1–1.4 Myr (Li *et al.*, 2008; Malinverno *et al.*, 2010), the event was characterized by the development of oxygen-depleted water columns across large parts of the global ocean and epicontinental shelf seas (e.g., Schlanger and Jenkyns, 1976; Weissert, 1989; Jenkyns, 1995; Pancost *et al.*, 2004; Föllmi *et al.*, 2006; van Breugel *et al.*, 2007). Ocean acidification, global temperature changes, accelerated hydrological cycling, and enhanced continental weathering rates have also been proposed to have occurred at that time (e.g., Erba, 2004; Ando *et al.*, 2008; Erba *et al.*, 2010, 2015; Bottini *et al.*, 2012, 2015; Hönisch *et al.*, 2012; Mutterlose *et al.*, 2014; Lechler *et al.*, 2015; Naafs and Pancost, 2016; Jenkyns, 2018). The various environmental perturbations are thought to have arisen from (and in some cases, contributed to) severe carbon-cycle disturbances. These perturbations are reflected by a series of carbon-isotope ($\delta^{13}\text{C}$) excursions documented from lower Aptian strata that record OAE 1a; typically interpreted via comparison to segments (C1–C7) in the stratigraphic $\delta^{13}\text{C}$ trends first recorded in Tethyan pelagic sedimentary archives (Menegatti *et al.*, 1998; see also Figure 1A, and Weissert, 1989; Jenkyns, 1995; Gröcke *et al.*, 1999; Ando *et al.*, 2008; Robinson *et al.*, 2008; Vickers *et al.*, 2016). Relatively stable $\delta^{13}\text{C}$ values spanning uppermost Barremian–lowermost Aptian strata (C1–C2) give way to a pronounced negative excursion in basal OAE 1a strata (C3), which is followed

by two distinct positive excursions (C4 and C6) that are locally separated by strata featuring stable carbon-isotope ratios higher than those of C2 (C5), and are succeeded by a continuation of high $\delta^{13}\text{C}$ values (C7) above the OAE 1a stratigraphic level (Menegatti *et al.*, 1998; see also Figure 1A).

The two positive $\delta^{13}\text{C}$ excursions that typically signify the C4 and C6 segments are thought to record enhanced rates of organic-matter burial in the widespread anoxic–euxinic water columns that characterized OAE 1a (e.g., Weissert, 1989; Menegatti *et al.*, 1998). Such organic-matter deposition is further evidenced by the preservation of organic-rich shales in several stratigraphic archives of the event worldwide (e.g., Schlanger and Jenkyns, 1976; Erba and Larson, 1998; Dumitrescu and Brassell, 2006; Hu *et al.*, 2012; Robinson *et al.*, 2017). Initially recognized in the Umbria–Marche Basin of Italy (Coccioni *et al.*, 1987), the organic-rich shale unit is named the Selli Level in that region, with sedimentary rocks of OAE 1a age (whether comprising organic-rich shales or otherwise) elsewhere around the world dubbed the Selli Level Equivalent (see Figure 1 and Study Areas section).

By contrast, the C3 negative $\delta^{13}\text{C}$ shift is attributed to a pronounced flux of isotopically light carbon to the ocean–atmosphere system that likely initiated the environmental perturbations associated with OAE 1a (e.g., Jahren *et al.*, 2001; Méhay *et al.*, 2009; Kuhnt *et al.*, 2011; Naafs *et al.*, 2016). The source of this isotopically light carbon remains debated. Several authors have linked the carbon emissions to the emplacement of one or more large igneous provinces (LIPs) during earliest Aptian times, particularly the Greater Ontong-Java Plateau (G-OJP; Figure 2; see e.g., Erba, 1994; Larson and Erba, 1999; Tejada *et al.*, 2009; Kuroda *et al.*, 2011; Bottini *et al.*, 2012; Erba *et al.*, 2015; Polteau *et al.*, 2016).

Geochemical modelling by Bauer *et al.* (2017) indicated that the emplacement of the G-OJP resulted in a geologically rapid six- to ten-fold increase in submarine volcanic activity during OAE 1a, and that such volcanism could have caused a fourfold rise in mantle carbon emissions ($\delta^{13}\text{C} \sim -6\text{‰}$; Gales *et al.*, 2020, and references therein). These emissions alone could have plausibly caused a similarly swift 3000 ppm increase in atmospheric $p\text{CO}_2$ levels and the 1.5–2‰ negative $\delta^{13}\text{C}$ excursion

typically documented in the C3 segment. However, based on $p\text{CO}_2$ trends reconstructed from the Cau section (Betic Cordillera, Spain), Naafs *et al.* (2016) argued that $p\text{CO}_2$ levels only rose gradually through the first part of OAE 1a and by <300 ppm during the C3 segment. In this case, a much smaller increase in carbon emissions, but with a very isotopically light composition ($\delta^{13}\text{C} < -10\text{‰}$), would have been required to cause the C3 negative excursion without greatly increasing atmospheric $p\text{CO}_2$ (Adloff *et al.*, 2020). Such parameters are inconsistent with a purely mantle-carbon source. Instead, this carbon could have been emitted following metamorphism of organic-rich sediments by intrusive sills during the emplacement of the High Arctic large igneous province (HALIP; Figure 2), or from the destabilisation of methane clathrates (e.g., Jahren *et al.*, 2001; Méhay *et al.*, 2009; Polteau *et al.*, 2016; Adloff *et al.*, 2020). This study investigates the geochemical records of volcanism related to the emplacement of the G-OJP and HALIP during the earliest Aptian and OAE 1a in order to determine the dominant style of magmatic activity operating during those times. This distinction might indicate whether or not a specific igneous province was the foremost source of carbon to the ocean–atmosphere system and likely the key trigger of the event.

1.1 Large Igneous Provinces emplaced during the latest Barremian and early Aptian

The G-OJP was an oceanic LIP consisting of several million cubic kilometres of igneous material (largely tholeiitic basalt) emplaced as intrusive and extrusive magma bodies into/onto the ocean crust of the western Pacific (Figure 2; see also Larson, 1991; Larson and Erba, 1999). The Ontong-Java Plateau alone has an immense volume of 10s of millions of cubic kilometres (possibly up to $44\text{--}57 \times 10^6 \text{ km}^3$; Gladchenko *et al.*, 1997). When other subsidiary plateaus thought to have initially formed as part of the G-OJP are included (e.g., the Manihiki and Hikurangi; Taylor, 2006; Hoernle *et al.*, 2010), the total volume of igneous material rises to $59\text{--}77 \times 10^6 \text{ km}^3$ (Kerr and Mahoney, 2007). The original province may have been even larger if a part of it was emplaced into/onto the now-subducted Farallon Plate, as has been previously suggested (Schlanger *et al.*, 1981; Larson, 1991). Thus, the G-OJP could have been an order of magnitude greater in size than the largest-known continental LIPs: the

Siberian Traps and Central Atlantic Magmatic Province, which were likely no more than $\sim 5 \times 10^6 \text{ km}^3$ each in volume (see review by Bond and Wignall, 2014). The average eruption rate on the G-OJP remains unknown. However, if Bauer *et al.*'s (2017) calculation of a six- to ten-fold increase in submarine volcanic activity during OAE 1a compared to pre-OAE background mid-ocean ridge volcanism is correct, and ridge basalt production during Barremian–Aptian times was similar to today ($\sim 20 \text{ km}^3/\text{yr}$; Cogné and Humler, 2006), then on average $>100 \text{ km}^3/\text{yr}$ of igneous material would have been emplaced on the G-OJP during OAE 1a. This average eruption rate is markedly higher than that proposed for any known continental LIP (e.g., Schoene *et al.*, 2019).

By contrast, Barremian–Aptian HALIP magmatism apparently consisted chiefly of subaerially erupted basalt flows and the intrusion of tholeiitic sills into organic-rich sedimentary rocks (Tegner *et al.*, 2011; Corfu *et al.*, 2013; Polteau *et al.*, 2016; Dockman *et al.*, 2018). The volume of HALIP igneous material emplaced during Barremian–Aptian times remains poorly constrained, but is thought to have been on the order of 100,000s of cubic kilometres (Tegner *et al.*, 2011; Polteau *et al.*, 2016; Dockman *et al.*, 2018), much smaller than the G-OJP but more comparable in volume to many other LIPs. However, the intrusion of organic-rich sediments by HALIP magmatic sills could have acted as an additional source of isotopically light carbon ($\delta^{13}\text{C} < -20 \text{ ‰}$) to the ocean–atmosphere system (Polteau *et al.*, 2016; c.f., Svensen *et al.*, 2004; McElwain *et al.*, 2005). By contrast, carbon emissions from the G-OJP would have been almost exclusively magmatic in origin, as that LIP was predominantly emplaced into comparatively volatile-depleted oceanic basalts.

Crucially, although there is some evidence from phreatomagmatic deposits dated to $\sim 120 \text{ Ma}$ for subaerial eruptions on the G-OJP during Barremian–Aptian times (Chambers *et al.*, 2004; Thordarson, 2004), the emplacement of that province into/onto the oceanic crust means that the great majority of volcanic activity associated with it is expected to have been submarine in nature. By contrast, most volatile emissions from HALIP subaerial basalts and thermogenic degassing should have reached the atmosphere. Previous studies have highlighted the fact that geochemical markers of LIP

volcanism in stratigraphic archives may be able to distinguish between these styles of magmatic processes, and also yield information on the proximity of the igneous activity (Kuroda *et al.*, 2011; Erba *et al.*, 2015). In particular, Percival *et al.* (2018) noted the differing degrees to which styles of volcanism can affect the likelihood of LIP emplacement and associated eruptions being recorded by two key proxies for these phenomena: mercury (Hg) concentrations and osmium- (Os-) isotope ratios (specifically $^{187}\text{Os}/^{188}\text{Os}$).

1.2 Sedimentary $^{187}\text{Os}/^{188}\text{Os}$ ratios as a marker of LIP emplacement during OAE 1a

Large igneous province emplacement can cause a change in the $^{187}\text{Os}/^{188}\text{Os}$ composition of the global ocean by acting as a major source of mantle-derived osmium, through either direct emission of the element during submarine volcanic/hydrothermal activity or weathering/alteration of juvenile LIP basalts (e.g., Cohen and Coe, 2002; Turgeon and Creaser, 2008). Importantly, the seawater residence time of osmium (on the order of 10s kyr today: Peucker-Ehrenbrink and Ravizza, 2000) means that the global ocean should feature a homogenous $^{187}\text{Os}/^{188}\text{Os}$ composition but still respond to geologically rapid changes in the sources to that inventory, except in hydrographically restricted basins with a very low basin–ocean water-mass exchange where the Os-isotope ratio might be dominated by local inputs (e.g., Paquay and Ravizza, 2012; Dickson *et al.*, 2015).

Primitive osmium derived from mantle or meteoritic material features $^{187}\text{Os}/^{188}\text{Os} \sim 0.13$ (Allègre *et al.*, 1999), whereas riverine osmium sourced from weathering of the continental crust is typically much more radiogenic (modern-day average riverine $^{187}\text{Os}/^{188}\text{Os} \sim 1.4$; Peucker-Ehrenbrink and Jahn, 2001). Consequently, a significant increase in the flux of mantle-derived Os from LIP activity to the global ocean, relative to riverine runoff of the element from weathering of the continental crust and the comparatively consistent mid-ocean-ridge and cosmogenic inputs, should result in a lower seawater $^{187}\text{Os}/^{188}\text{Os}$ ratio throughout the open ocean. This hydrogenous Os-isotope signature is

recorded in seafloor sediments, which can preserve past seawater compositions as long as the sedimentary system remains closed with respect to rhenium and osmium following deposition (Cohen *et al.*, 1999).

In all previously studied records of OAE 1a, a pronounced shift is observed in the recorded seawater Os-isotope ratio ($^{187}\text{Os}/^{188}\text{Os}_{(i)}$) towards very unradiogenic compositions (typically <0.2) around the base of the Selli Level or equivalent strata deposited during OAE 1a, together with an increase in sedimentary Os concentrations (Tejada *et al.*, 2009; Bottini *et al.*, 2012; Adloff *et al.*, 2020; see also Figure 1B). These unradiogenic $^{187}\text{Os}/^{188}\text{Os}_{(i)}$ compositions and high Os concentrations generally continue up the stratigraphy through the entire Selli Level (or equivalent), and are thought to document intense LIP volcanism that acted as a source of osmium to the global ocean through one or both of submarine hydrothermal emissions of the element and erosion/alteration of the juvenile basalts formed during the volcanic activity (Tejada *et al.*, 2009; Bottini *et al.*, 2012; Adloff *et al.*, 2020). However, Tethyan records of OAE 1a also document a brief rebound in Os-isotope ratios to higher values in basal Selli Level (or equivalent) strata, potentially highlighting a transient spell of enhanced continental weathering and associated flux of radiogenic Os at the onset of the event that temporarily overprinted the unradiogenic signature (Tejada *et al.*, 2009; Bottini *et al.*, 2012). This transient pulse of enhanced continental weathering early in OAE 1a is supported by strontium- and lithium-isotope excursions (Jones and Jenkyns, 2001; Lechler *et al.*, 2015).

1.3 Sedimentary Hg concentrations as a marker of LIP volcanism during OAE 1a

Volcanic eruptions represent one of the largest natural sources of mercury to the Earth's surface in the present day (Pyle and Mather, 2003; Bagnato *et al.*, 2007). Mercury is chiefly emitted as a gaseous elemental species that typically has a residence time of 0.5–2 years in the stratosphere, enabling worldwide distribution before the element is ultimately deposited in sediments (Schroeder and Munthe, 1998; Ericksen *et al.*, 2003; Selin *et al.*, 2009). The global distribution of volcanic mercury has led

several studies of geological events associated with LIPs to utilise sedimentary concentrations of the element as a proxy for the volcanism (see reviews by Grasby *et al.*, 2019; Percival *et al.*, 2021). This approach includes normalising sedimentary mercury concentrations against total organic carbon (TOC) content to account for the association of the element with organic compounds when it is deposited in sediments (Sanei *et al.*, 2012, and references therein). Thus, peaks in sedimentary Hg/TOC ratios are generally interpreted as reflecting an increased input of Hg to the environment from an external source, such as volcanism or wildfires, the latter of which is also known to cause peaks in sedimentary Hg and Hg/TOC values in modern settings (e.g., Daga *et al.*, 2016).

However, in euxinic settings where free sulphides precipitate in the water column, Hg may be deposited with that phase rather than organic matter (Shen *et al.*, 2019a; Shen *et al.*, 2020). Alternatively, in a very well-oxygenated environment, featuring limited burial of both phases, mercury might be adsorbed on to clays (Kongchum *et al.*, 2011; Shen *et al.*, 2020). Even in settings where Hg contents follow those of TOC, a change in the type of organic matter (e.g., from marine bacterial to terrestrial detrital), or a large influx of organic material from a new source, could alter the Hg/TOC ratio if the affinity of mercury for the various kinds of organic material varies (see Hammer *et al.*, 2019; Them *et al.*, 2019). Therefore, robustly demonstrating a global-scale perturbation to the mercury signature caused by volcanism is dependent on documenting enrichment of the element in stratigraphic archives that cover a wide range of geographic areas, and for which the depositional environment and burial history are known.

To date, three stratigraphic archives of OAE 1a have been investigated for mercury and Hg/TOC trends by Charbonnier and Föllmi (2017), all of them representing palaeoenvironments from the north-westernmost part of the Tethyan realm: La Bédoule (South Provençal Basin, SE France), Glaise (Vocontian Basin, SE France), and Roter Sattel (Briançonnais Domain, Switzerland). This last record has been shown as being rather thermally mature (Charbonnier *et al.*, 2018a), potentially altering the TOC content and inflating measured Hg/TOC ratios to above those from the time of deposition (as shown for other Cretaceous records by Charbonnier *et al.*, 2020). Nonetheless, Charbonnier and Föllmi

(2017) reported increased Hg and Hg/TOC values that were ascribed to G-OJP volcanic activity during OAE 1a (see also Supplementary Figure 1). Interestingly, Barremian–Aptian boundary records from the northwest Tethyan area have also been hypothesized as recording an earlier episode of volcanism associated with that LIP, which took place significantly prior to OAE 1a (Charbonnier *et al.*, 2018b).

1.4 Study aims

Whilst mercury-cycle perturbations from Barremian–Aptian times (including OAE 1a) have been reported from the northwest Tethyan area, and linked to volcanism on the G-OJP, it remains unclear whether these disturbances truly represent a global volcanic signal or local influxes of mercury to that specific region. In this context, it is notable that mercury emitted from modern submarine volcanic systems appears to be efficiently scavenged, limiting dispersal of the element from such sources to areas relatively proximal to the point(s) of origin (within 100s km; Bowman *et al.*, 2015). Indeed, prior investigations of the latest Cenomanian OAE (OAE 2; ~94 Ma), which has also been linked with submarine LIP volcanism during oceanic-plateau emplacement (e.g., Turgeon and Creaser, 2008), have shown that most studied records of that event do not feature Hg enrichments or elevated Hg/TOC ratios, except perhaps for sites proximal to LIPs (Scaife *et al.*, 2017; Percival *et al.*, 2018).

Consequently, analyses of stratigraphic archives of OAE 1a from around the world are needed in order to determine whether there was global-scale Hg-cycle perturbation during that event, or localized disturbances unrelated to magmatism. Furthermore, a global perspective of the mercury cycle will help to elucidate whether any volcanic fluxes of mercury were largely derived from G-OJP or HALIP activity. If volatile emissions during OAE 1a were primarily associated with submarine LIP activity of the G-OJP, sedimentary mercury enrichments correlative with the Os-isotope evidence of volcanism would likely be recorded in Pacific sites proximal to that source, but potentially nowhere else due to the limited dispersal range of the element in the marine realm. By contrast, mercury fluxes

from subaerial eruptions and/or thermogenic emissions related to the HALIP should certainly be documented in the Arctic, and might also be documented in sites around the world due to those magmatic processes being more likely to emit volatiles directly to the atmosphere.

Here, new mercury data are presented from six records of latest-Barremian–early Aptian age, including OAE 1a (Figure 2): DSDP Site 463 (Mid-Pacific Mountains), the Cismon core (Belluno Basin, Italy), the Poggio le Guaine core (Umbria–Marche Basin, Italy), the Notre-Dame-de-Rosans section (Vocontian Basin, SE France), the DH-1 Longyearbyen core (Boreal Basin, Svalbard), and the Petrobras Well D (Sergipe-Alagoas Basin, NE Brazil). New Os-isotope data are also presented from the Poggio le Guaine core. These sequences include the first OAE 1a records from outside the Tethyan region that have been studied for mercury, offering a more global perspective on any Hg-cycle perturbations during that time. Crucially, these study areas include three sites where stratigraphic Hg and Os-isotope trends can be directly correlated (DSDP Site 463 and the Cismon and Poggio le Guaine cores). Additionally, the Mid-Pacific Mountain and Arctic sites would have been relatively proximal to the G-OJP and HALIP, respectively. Comparing these new mercury and osmium-isotope profiles with previously published datasets, and correlating trends in the two proxies amongst records where both have been studied, will give new insights on the dominant style of volcanic activity that influenced the global Hg cycle during OAE 1a and could potentially identify the LIP that was the primary trigger of that event.

2 STUDY AREAS

2.1 DSDP Site 463 (Mid-Pacific Mountains, W Pacific Ocean)

DSDP Site 463, drilled in the Mid-Pacific Mountains in 1978, records a large part of the uppermost Barremian to lower Aptian stratigraphic interval (Thiede *et al.*, 1981). The lithology

generally consists of pelagic limestones with some chert-rich intervals (Mélières *et al.*, 1981). There is a switch to more clay-rich marlstones between ~625–615 mbsf that marks the OAE 1a stratigraphic interval (Thiede *et al.*, 1981; Sliter, 1989). However, black shales akin to those observed in most Tethyan archives are largely absent from this site and only appear in upper Selli Level Equivalent strata, with a modest increase in TOC content (to 1.5 wt%, *this study*; although previous works have reported values locally up to 7–8 wt%; Thiede *et al.*, 1981; van Breugel *et al.*, 2007; Bottini *et al.*, 2012). Age constraints (including the position of the Barremian–Aptian boundary) are based largely on magneto- and biostratigraphy (Tarduno *et al.*, 1989). Several studies have investigated the Barremian–Aptian carbon-isotope trends at DSDP Site 463 (e.g., Price, 2003; Ando *et al.*, 2008; Bottini *et al.*, 2012), identifying the C2–C7 segments that can be used to define the Selli Level Equivalent strata deposited during OAE 1a. Osmium-isotope trends and trace-metal enrichments have been interpreted as evidence for intense volcanic activity during Barremian–Aptian times (particularly before and during OAE 1a), with the volcanism generally attributed to the nearby G-OJP (Bottini *et al.*, 2012; Erba *et al.*, 2015). Volcanic eruptions proximal to DSDP Site 463 are supported by sporadic preservation of thin tuffaceous layers locally preserved within the Barremian–Aptian sediments, particularly within the Selli Level Equivalent (Hein and Vanek, 1981; Vallier and Jefferson, 1981; Thiede *et al.*, 1982). The provenance of these tuffs remains unknown, but given the proximity of the Mid-Pacific Mountains to the G-OJP, eruptions on that volcanically active LIP would be a plausible source.

2.2 Cismon core (Belluno Basin, Italy)

The Cismon core was drilled in the Southern Alps north-west of Treviso (Italy) in 1995, and is one of the best-studied latest Barremian–Aptian Tethyan records (Erba and Larson, 1998). The core largely consists of pale-coloured pelagic carbonates deposited on the slope of the Belluno Basin. However, the Selli Level Equivalent is marked by a clear lithological change to organic-rich marlstones and shales interbedded with sporadic radiolarian-rich beds (Erba and Larson, 1998). The increase in

TOC, together with elevated sulphur contents and preservation of the biomarker isorenieratane in some Selli Level Equivalent beds, strongly supports the development of at least periodically euxinic conditions in the Belluno Basin during OAE 1a (van Breugel *et al.*, 2007; Bottini *et al.*, 2012). Magneto-, bio-, and carbon-isotope stratigraphy provide excellent temporal constraints, with all the $\delta^{13}\text{C}$ excursions and C1–C8 segments well preserved (Menegatti *et al.*, 1998; Erba *et al.*, 1999; Channell *et al.*, 2000). A pronounced decline in the abundance of nannoconids has been documented just below the Barremian–Aptian boundary, with a further reduction (to almost nothing) of these nannofossils near the base of the Selli Level Equivalent (Erba, 1994). These changes in the fossil record highlight the biotic impact of the environmental perturbations that took place prior to and during OAE 1a (e.g., Bralower *et al.*, 1994; Erba, 1994; Erba and Tremolada, 2004; Erba *et al.*, 2010). Age modelling of lower Aptian strata from the Cismon core have indicated dates for the Barremian–Aptian transition and OAE 1a that overlap with G-OJP basalt ages (see Malinverno *et al.*, 2012; Erba *et al.*, 2015). Furthermore, both osmium-isotope trends (see above) and enrichments in several trace metals of probable mafic derivation in Barremian–Aptian strata provide direct evidence of LIP activity at that time (Bottini *et al.*, 2012; Erba *et al.*, 2015).

2.3 Poggio le Guaine core (Umbria–Marche Basin, Italy)

The Poggio le Guaine (PLG) core was drilled in 2010 in the Northern Apennines at a site 6 km to the west of the city of Cagli (Coccioni *et al.*, 2012), close to a previously studied lower Aptian outcrop that includes sediments of OAE 1a age deposited as the Selli Level *sensu stricto* (e.g., Lowrie *et al.*, 1980; Coccioni *et al.*, 1987, 1990; Baudin *et al.*, 1998). Like the outcrop section, the core represents a well-preserved and apparently continuous Aptian–Albian succession that records a pelagic environment in the Umbria–Marche Basin of the north-western Tethyan area. The lithology is dominated by white and grey nannofossil-foraminiferal pelagic limestones, with rare cherts, radiolarian-rich beds, and green limestones (Coccioni *et al.*, 2012; Savian *et al.*, 2016). Stratigraphic age constraints on the position of the Barremian–Aptian boundary are based on magnetostratigraphy and calcareous planktonic

foraminiferal biostratigraphy (Coccioni *et al.*, 2012; Savian *et al.*, 2016). Intercalated organic-rich shales and radiolarian-rich beds, an overall relative elevation in TOC contents, and a negative (C3) and recovery/broad positive excursion (C4–C6) in carbonate $\delta^{13}\text{C}$ ratios all define the Selli Level (89.24–91.29 m; Coccioni *et al.*, 2012; Savian *et al.*, 2016; *this study*). However, within the OAE 1a strata there is a black-shale unit containing insufficient carbonate for carbon-isotope analysis, leaving a gap in the $\delta^{13}\text{C}$ trends that hinders precise placement of the C4–C5 and C5–C6 boundaries (~89–91 m).

2.4 Notre-Dame-de-Rosans (Vocontian Basin, SE France)

The Vocontian Basin was one of a number of large epicontinental depocentres located in the north-western area of the Cretaceous Tethys Ocean, formed by tectonic processes related to the opening of the Bay of Biscay (e.g., Hibschi *et al.*, 1992), with basinal clay-rich calcareous hemipelagic sediments preserved today in south-eastern France (Bréhéret, 1997). The Notre-Dame-de-Rosans section provides an excellent record of OAE 1a in the Vocontian Basin, comprising interbedded clay-rich calcareous marls and fine-grained turbidites (Giraud *et al.*, 2018). The stratigraphy can be correlated with other archives from that region, and elsewhere, based on biostratigraphic constraints, its carbon-isotope record (clearly documenting the C2–C7 segments), and the preservation of less calcareous, darker coloured, TOC-enriched grey marls in the upper part of the Selli Level Equivalent (Giraud *et al.*, 2018), locally named the Niveau Goguel (Bréhéret, 1998). This organic matter is immature and appears to be largely composed of marine algal/bacterial material, but potentially with some contribution from degraded/terrestrially derived debris (Giraud *et al.*, 2018). Based on the identification of <6 µm framboidal pyrite and cyanobacterial biomarkers in the Niveau Goguel strata of the nearby Les Sauzeries section (<50 km away), it has been inferred that anoxic–euxinic settings developed during the latter part of OAE 1a (Ando *et al.*, 2013; Giraud *et al.*, 2018). However, such conditions were likely intermittent, with the turbidite flows reventilating the marine environment (Caillaud *et al.*, 2020).

2.5 DH-1 core, Longyearbyen (Boreal Basin, Svalbard, Norway)

The western part of Svalbard records a very near-shore shallow-marine palaeoenvironment in an epicontinental basin, with a lithology consisting of mudstone–siltstone beds, fluvial–marginal marine sandstone lenses, and coals (Midtkandal *et al.*, 2016; Vickers *et al.*, 2016). Macroscopic higher-plant debris in DH-1 core samples supports a dominantly terrestrial source of organic matter, further evidenced by low measured hydrogen index (HI) values, although the low HI could partly/completely result from the high thermal maturity of the sediments (Midtkandal *et al.*, 2016). A limited quantity of marine palynomorphs allows for dinoflagellate biostratigraphy, from which a broadly Barremian–Aptian age for the interval of the DH-1 core studied here has been determined (Midtkandal *et al.*, 2016). A negative $\delta^{13}\text{C}$ excursion and positive shift immediately stratigraphically above it (150.47–133.37 m) are thought to be equivalent to the C3 and C4–C6 segments, respectively, and have been interpreted as marking the Selli Level Equivalent strata in the core (Midtkandal *et al.*, 2016). Further subdivision of the C4–C6 segments is not possible due to the low resolution of the $\delta^{13}\text{C}$ dataset. Interestingly, TOC contents decrease to an average of 1.8 wt% within the Selli Level Equivalent, compared to mean quantities of 3.8 wt% and 3.3 wt% in sediments stratigraphically above and below, respectively (Midtkandal *et al.*, 2016). For this study, mercury analyses were limited to mudstone layers, avoiding sandstone/coal beds, in order to maintain relative consistency in terms of the lithology and organic-matter content of the studied samples, as previous works have shown that major lithological variations can strongly influence Hg concentrations and Hg/TOC variations independently of any potential external source (e.g., Percival *et al.*, 2018).

2.6 Petrobras Well D (Sergipe-Alagoas Basin, NE Brazil)

The Sergipe-Alagoas Basin was one of a number of rift-basins along the eastern and southern part of Brazil that formed during the Early Cretaceous as a result of the opening of the South Atlantic

Ocean (Chaboureaud *et al.*, 2013, and references therein). The Petrobras Well D was drilled through the Muribeca and Riachuelo Formations of the basin, consisting of sandy and conglomeratic siliciclastics interbedded with siltstones and mudstones, the last of which are locally calcareous. Taken together, the stratigraphic sequence is interpreted as having been deposited in a continental–coastal setting that was initially dominated by fluvio-deltaic systems, but gradually transitioned towards lacustrine/lagoonal settings due to continuing basin subsidence as rifting of the South Atlantic proceeded (Tedeschi *et al.*, 2020). Elsewhere in the Sergipe-Alagoas Basin, the Riachuelo Formation has been dated as late Aptian in age on the basis of planktonic foraminiferal biostratigraphy (e.g., Koutsoukos *et al.*, 1992), with the underlying Muribeca Formation generally accepted as also having been deposited (earlier) in the Aptian (Tedeschi *et al.*, 2020). Consequently, a series of pronounced carbon-isotope excursions near the bottom of the Muribeca Formation in the Petrobras Well D core has been interpreted as marking the Selli Level Equivalent, with a negative excursion overlain by two positive shifts interpreted as the C3 and C4–C6 segments, respectively (Tedeschi *et al.*, 2020). TOC contents are variable, ranging from <0.1 wt% up to 5.2 wt%, with mean values highest in the postulated C5 strata, and primarily composed of detrital terrestrial organic matter that has locally been oxidized, based on the determined hydrogen and oxygen indices and the nature of the recorded palaeoenvironment (Tedeschi *et al.*, 2020).

3. METHODS

Mercury data for all records were generated using a RA-915 Portable Mercury Analyzer with PYRO-915 Pyrolyzer, Lumex, at the University of Oxford (UK). Analyses were carried out following the methodology in Percival *et al.* (2017), with at least two analyses conducted for each sample. Two reference materials were utilized as standards for machine calibration and drift check throughout a set of analyses: NIMT/UOE/FM/001 – Inorganic Elements in Peat (169 ppb Hg) and NIST-SRM2587 – Trace Elements in Soil Containing Lead from Paint (290 ppb Hg). Analytical uncertainty based on repeated measurements of the reference materials was ± 15 ppb. Concentrations of other metals in the DH-1 core samples were measured by ICP-AES at Imperial College London (UK) following

preparation by lithium metaborate fusion and hydrofluoric/perchloric acid digestion, after the methods in Neumann *et al.* (2013).

New TOC data were generated by Rock-Eval 6 analysis for samples from DSDP Site 463, the Cismon core, and Notre-Dame-de-Rosans, at the University of Oxford, after the methodology of Behar *et al.* (2001). Repeated measurements of an internal mudrock standard SAB134 (calibrated to the International reference material IFP 160000) were used to assess analytical accuracy and repeatability, and yielded an average value of 2.81 ± 0.07 wt%, consistent with long-term measurements for the laboratory (2.87 ± 0.11 wt%; Storm *et al.*, 2020), and indicating analytical uncertainty better than 0.1 wt% (1σ). New TOC data for PLG core samples were determined on a Strohlein Coulomat 702 at the University of Oxford, using the procedure in Jenkyns (1988). TOC contents have been previously determined using Rock Eval and Leco SC-632 instruments for all samples from the DH-1 core and Petrobras Well D analyzed for mercury in this study, at the Institute for Energy Technology, Kjeller (Norway) for the DH-1 core (Midtkandal *et al.*, 2016), and at the Universities of Oxford and Universidade do Estado do Rio de Janeiro for Petrobras Well D (Tedeschi *et al.*, 2020). The new data from the Cismon core were combined with published values that were generated at the Open University (UK) using a Leco CNS-2000 elemental analyser (Bottini *et al.*, 2012).

New osmium-isotope data were determined for ten samples from the PLG core following the methodology outlined in Kendall *et al.* (2015), with eight samples taken from the Selli Level, and two others from beneath the base of it. Sample preparation utilized Carius-tube digestion with $\text{Cr}^{\text{VI}}\text{O}_3$ - H_2SO_4 , with subsequent Os purification using established solvent extraction (by chloroform) and microdistillation techniques (Selby and Creaser, 2003). Rhenium purification was carried out with solvent extraction using sodium hydroxide and acetone, and subsequent anion exchange chromatography (Cumming *et al.*, 2013). Isotopic compositions and concentrations of rhenium and osmium were determined by isotope dilution and negative thermal ionisation mass spectrometry (N-TIMS) on a Thermo Triton instrument at the Department of Earth and Atmospheric Sciences, University of Alberta (Canada). Total procedural blanks for osmium and rhenium were 0.3 and 15 pg, respectively,

whilst the $^{187}\text{Os}/^{188}\text{Os}$ composition of the blanks was 0.20. In-house standard solutions for osmium (AB2; see e.g., Selby, 2007; Finlay *et al.*, 2010) and rhenium (ICP-MS standard rhenium solution of normal isotopic composition) yielded values in agreement with previous studies (van Acken *et al.*, 2013; Kendall *et al.*, 2015): $^{187}\text{Os}/^{188}\text{Os}$ of 0.10684 ± 0.00015 (1σ) for osmium, and $^{185}\text{Re}/^{187}\text{Re}$ of 0.59778 ± 0.00077 (1σ) for rhenium.

The past seawater composition at the time of deposition ($^{187}\text{Os}/^{188}\text{Os}_{(i)}$) is determined from the modern-day $^{187}\text{Os}/^{188}\text{Os}$ ratio of a sedimentary rock sample using its age and its Re and Os concentrations to account for the post-depositional decay of rhenium (^{187}Re) to ^{187}Os (Cohen *et al.*, 1999). The osmium concentration of a sedimentary rock at the time of its deposition is determined from the modern-day osmium concentration after accounting for the post-depositional decay of ^{187}Re to ^{187}Os , by using the difference between the measured modern-day $^{187}\text{Os}/^{188}\text{Os}$ ratio and the calculated $^{187}\text{Os}/^{188}\text{Os}_{(i)}$ value, together with the ^{192}Os content of the rock and the known natural $^{192}\text{Os}/^{188}\text{Os}$ isotope ratio (see Supplementary Text).

4. RESULTS

4.1 Os-isotope and osmium concentration data from the PLG core

Following correction of the measured modern-day Os-isotope ratio for decay of rhenium since deposition at 120 Ma, the recorded $^{187}\text{Os}/^{188}\text{Os}_{(i)}$ values show a clear shift from ~ 0.6 to ~ 0.2 in the basal Selli Level strata (Figure 3). There is also a notable increase in the calculated $[\text{Os}_{(i)}]$ concentrations across that horizon, from 149 ppt in the stratigraphically lowest analyzed sample to a maximum of 3719 ppt in the middle of the Selli Level. These trends are broadly consistent with osmium trends from Gorgo a Cerbara, Cismon (both Italy), DSDP Site 463 (Pacific), and Cau (Spain) reported by previous studies (Tejada *et al.*, 2009; Bottini *et al.*, 2012; Adloff *et al.*, 2020). Interestingly, the transient shift to more

radiogenic $^{187}\text{Os}/^{188}\text{Os}_{(i)}$ values documented from other Tethyan records (Cismon and Gorgo a Cerbara; Tejada *et al.*, 2009; Bottini *et al.*, 2012; see Figure 1) is not observed in the PLG data. This lack of $^{187}\text{Os}/^{188}\text{Os}_{(i)}$ spike in the PLG core may result from the absence of data from below the Selli Level at that site (Figure 3). Alternatively, the $^{187}\text{Os}/^{188}\text{Os}_{(i)}$ spike may not be captured by the PLG dataset due to its relatively low-resolution, or the presence of a small hiatus/condensed layer at the base of the Selli Level, although there is no sedimentological evidence for such a stratigraphic gap.

4.2 Hg concentration and Hg/TOC ratio data

At DSDP Site 463, there is a clear increase in Hg content from the average of 16.4 ppb below the Selli Level Equivalent to a mean of 101 ppb within it, with a first increase up to 168.5 ppb in C3 (625.28–623.96 mbsf) and a second peak up to 471.5 ppb in the C4–lowest C5 segments (622.22–620.10 mbsf), before returning to much lower (mean 18.4 ppb) values in sediments above the Selli Level Equivalent (Figure 4A). By contrast, the TOC contents of DSDP Site 463 samples that were also measured for mercury are relatively consistent, and low: typically <0.5 wt%, apart from for three samples in the middle of the Selli Level Equivalent that have values close to or above 1 wt%. Interestingly, no sample measured in this study had TOC contents of 7–8 wt% as reported for some stratigraphic layers at DSDP Site 463 by previous works (see section 2.1). Consequently, the two increases in Hg concentrations are largely reproduced by Hg/TOC ratios, with peaks up to 802 ppb/wt% and 689 ppb/wt% in C3 and lowest C5 strata, respectively (Figure 4A). Crucially, both peaks greatly exceed the range of error of background samples, confirming that they do not result from analytical uncertainty. A small number of samples have a TOC content that is too low to confidently interpret Hg/TOC ratios (Hg/TOC ratios based on TOC contents < 0.2 wt% are generally deemed unreliable due to the high percentage error in the TOC measurement: see Grasby *et al.*, 2016). However, the inclusion or exclusion of these data does not greatly affect the recorded stratigraphic trends.

Hg concentrations in the Cismon core are extremely variable throughout the studied interval, ranging between 3.7–334 ppb with a number of peaks: either side of the Barremian–Aptian boundary (at 34.21 m and 27.85 m), within the C3 to C4 strata (~23 m), and again in the C6 segment between 19.87–18.83 m (Figure 4B). TOC contents of samples below the Selli Level Equivalent are typically very low (only three samples exceed 0.2 wt%), resulting in highly variable Hg/TOC values between 113–1637 ppb/wt% that also show peaks either side of the Barremian–Aptian boundary, although interpreting these data is greatly hindered due to the normalisation by extremely low TOC contents. By contrast, the typically higher TOC contents within the Selli Level Equivalent result in generally lower, though still variable, ratios between 7.9–468 ppb/wt% (Figure 4B). However, the C3–C4 peak in Hg concentrations is only reproduced by a two data-point peak in Hg/TOC, with no increase in Hg/TOC ratios in the C6 segment.

Similarly to the Cismon core, the PLG record features rather variable sedimentary Hg concentrations between 1.4–201 ppb, with a number of peaks below the Selli Level and another peak within the lower part of the C4–C6 strata within it (Figure 4C). Concentrations across the Barremian–Aptian boundary and above the Selli Level are particularly low (averaging 9.9 ppb). TOC contents increase markedly from typically <0.5 wt% below the Selli Level to values in excess of 2 wt% within it; one sample reaching 10.7 wt% (Figure 4C). The various peaks in Hg are maintained to some degree following normalisation against TOC, with three peaks of between 200–600 ppb/wt%: one at 93.8–93.6 m, a second at 92.2 m (both below the OAE 1a horizon), and finally at 90.4 m (lowest C4–C6 strata), albeit consisting of just one or two data points (Figure 4C). However, it should be noted that several PLG Hg data points are normalized against low (but >0.2 wt%) TOC contents, creating a high level of uncertainty in the Hg/TOC stratigraphic trend. Many of the PLG Hg/TOC peaks do not significantly exceed this range of error; thus, they cannot be unambiguously interpreted as marking an external influx of mercury.

Hg concentrations are consistently low through most of the Notre-Dame-de-Rosans strata (averaging 28.6 ppb), apart from a peak up to 156.5 ppb (mean 60.0 ppb) spanning the uppermost C3,

all of C4, and lower C5 segments (18.8–24.9 m; Figure 4D). Newly measured TOC contents in the samples analyzed for mercury show comparable trends to those previously published by Giraud *et al.* (2018), averaging approximately 0.5 wt% throughout most of the studied record, except in the C6 upper part of the Selli Level Equivalent (the Niveau Goguel), where values rise to between 1–2 wt% (Figure 4D). Consequently, the peak in Hg concentrations largely remains following normalisation by TOC, with an increase in Hg/TOC ratios up to 333 ppb/wt% in C4 strata, compared to consistently lower values averaging 64 ppb/wt% throughout the rest of the studied interval.

Hg concentrations are variable throughout the studied interval of the DH-1 core, but show a systematic increase across the Selli Level Equivalent. The basal (C3) strata are marked by a peak up to 202 ppb at 150.47 m, which is succeeded by a broader increase averaging 73.8 ppb across the upper C4–C6 segments (144.3–136.02 m), compared to much lower contents that are typically <10 ppb throughout the rest of the record (Figure 4E). When normalized against the TOC contents of these samples (previously published by Midtkandal *et al.*, 2016), the C3 peak in Hg largely disappears, but the elevated Hg contents across C4–C6 strata are reflected by a rise in average Hg/TOC values to 40 ppb/wt% in these strata, compared to 12.1 ppb/wt% for the rest of the record (Figure 4E).

Hg concentrations are consistently very low (averaging 13.9 ppb) throughout the studied interval of the Petrobras Well D, and show no increase across the postulated Selli Level Equivalent (Figure 4F). As for the DH-1 core, TOC contents of these samples have been previously published (Tedeschi *et al.*, 2020), with a marked increase from <0.1 wt% below the OAE 1a level to generally between 1–3 wt% (up to a maximum of 5.22 wt%) within it. Consequently, Hg/TOC ratios are generally also very low (averaging <20 ppb/wt%) with a few higher values near the base of the studied interval caused by low TOC contents (Figure 4F). There is one sample (from 201.43 m) with anomalously high Hg concentrations and Hg/TOC ratios of 373 ppb and 158 ppb/wt%, respectively, but this is significantly above the top of the Selli Level Equivalent.

5. DISCUSSION

5.1 Tethyan Hg-cycle disturbances prior to OAE 1a

Volcanic activity related to G-OJP emplacement has been previously proposed as having occurred during latest Barremian times, based on enrichments in mercury and other trace metals across the Barremian–Aptian boundary, especially in Tethyan stratigraphic archives (Erba *et al.*, 2015; Charbonnier *et al.*, 2018b). Some increase in submarine volcanism and/or basalt–seawater interaction might also be registered by a small shift towards mantle compositions in Pb and Os isotopes across the Barremian–Aptian boundaries of the Shatsky Rise and Cismon records, respectively (Kuroda *et al.*, 2011; Bottini *et al.*, 2012). It has been further suggested that this G-OJP volcanism contributed to the decline in nannoconid fauna during the Barremian–Aptian transition (Erba *et al.*, 2015). Whilst Hg concentrations and Hg/TOC ratios are highly variable in pre-OAE 1a strata from the Cismon and PLG cores, peaks around the Barremian–Aptian boundary (and particularly strata of the magnetic chron CM0) might support a mercury-cycle disturbance in the Tethyan region at that time (Figure 4B–C). However, interpretation of the Hg/TOC ratios for both the Cismon and PLG cores is greatly hindered by the very low TOC contents of most samples (and attendant large range of uncertainty) from strata below the Selli Level or equivalent. Indeed, given the relatively low organic-matter and (in the case of Cismon) sulphur contents in Barremian–Aptian boundary sediments (Figure 4B–C; Supplementary Figure 2B), a lithological control on mercury deposition, whereby the element is associated with clay minerals, is likely for these strata. This conclusion is reinforced by the absence of Hg peaks in strata above the PLG Selli Level, when argillaceous layers (which make up much of the Selli Level and are interbedded with limestones beneath it) discontinue, leaving only calcareous lithologies.

Even if there were one or more Hg-cycle perturbations (volcanically stimulated or otherwise) in the Tethyan realm during the Barremian–Aptian transition prior to OAE 1a, there is no evidence that

such phenomena were occurring outside of this region. Hg concentrations and Hg/TOC ratios remain relatively low throughout the (admittedly incomplete) strata below the Selli Level Equivalent at DSDP Site 463 (Figure 4A). Given how proximal this Mid-Pacific Mountains site was to the G-OJP, if volcanism on that LIP were capable of dispersing sufficient Hg to reach the northwest Tethys, the expectation would be for it to be recorded in more proximal sedimentary records as well. Nor can the absence of Barremian–Aptian Hg enrichment at DSDP Site 463 be attributed to overprinting by excess TOC, as the Hg concentrations themselves largely remain low. Thus, whilst activity on the G-OJP during the latest Barremian is not discounted as the cause of the nannoconid decline, if the LIP was volcanically active at that time then it apparently did not perturb either the regional or global mercury cycle significantly. Volcanism on the north-eastern Tethyan margin has been suggested as a potential cause of Hg peaks in Valanginian sedimentary records from the northwest Tethys (Charbonnier *et al.*, 2017), but there is no clear indication that such eruptions took place during latest Barremian to early Aptian times. Thus, without evidence of north-western Tethyan eruptions or G-OJP mercury emissions during the Barremian–Aptian transition, the Hg/TOC variations documented stratigraphically below the Selli Level (or equivalent strata) in the Cismon and PLG cores cannot be conclusively linked to volcanism.

5.2 Evidence for submarine G-OJP volcanism at the onset of OAE 1a

The shift in $^{187}\text{Os}/^{188}\text{Os}_{(i)}$ values towards unradiogenic compositions in basal Selli Level (C3) strata of the PLG core matches published Os-isotope stratigraphic trends from other sites in the Tethys and Pacific (Figure 5). This similarity supports the commencement of intense LIP volcanism, or at least some form of basalt–seawater interaction, during the onset of OAE 1a. There is a clear correlation between the $^{187}\text{Os}/^{188}\text{Os}_{(i)}$ shift and the increased Hg and Hg/TOC values at DSDP Site 463; however, no such relationship is documented in the Cismon or PLG cores (Figure 5). Whilst no $^{187}\text{Os}/^{188}\text{Os}_{(i)}$ data exist for the other six sites studied for mercury here and by Charbonnier and Föllmi (2017), it can be seen that although most of those locales record some enrichment(s) in sedimentary mercury, none of

633 them feature a clear peak in Hg and Hg/TOC in the C3 segment comparable to that in coeval strata of
634 DSDP Site 463 (Figure 4 and Supplementary Figure 1).

635
636 Given that by far the clearest sedimentary mercury enrichment during the onset of OAE 1a is
637 at DSDP Site 463, it is possible that this single-site peak results from a lithological change in that
638 archive, such as increased clay content or burial with pyrite (c.f., Shen *et al.*, 2020). Alternatively, it
639 may reflect a local input of Hg from increased wildfire activity/runoff of terrestrial organic matter (c.f.
640 Daga *et al.*, 2016; Grasby *et al.*, 2017; Them *et al.*, 2019). However, the C3 Hg enrichment at DSDP
641 Site 463 does not correlate with an increase in total clay or pyrite content (Supplementary Figure 2A),
642 ruling out an association between mercury and such phases, and thereby discounting lithological/redox
643 changes as the cause of the Hg/TOC increase. Organic-matter oxidation/degradation has been reported
644 from the DSDP Site 463 Aptian record, but van Breugel *et al.* (2007) noted that the sediments from the
645 basal part of the Selli Level Equivalent are less thermally mature than the rock layers stratigraphically
646 below and above, making it unlikely that the C3 Hg/TOC peak merely results from post-depositional
647 TOC depletion (c.f., Charbonnier *et al.*, 2020). Both marine and terrestrially derived organic matter are
648 known to be present in Selli Level Equivalent sediments of DSDP Site 463, but an increased abundance
649 in terrestrial material specifically in the C3 Segment has not been robustly established (Mélières *et al.*
650 1981; Dean *et al.*, 1984; van Breugel *et al.*, 2007).

651
652 Notably, however, the Hg and Hg/TOC increase at the base of the Selli Level Equivalent
653 stratigraphically correlates with the appearance of abundant tuffaceous layers (Figure 6). Thus, it is
654 likely that the mercury peaks at DSDP Site 463 were caused by nearby volcanic activity proximal to
655 the G-OJP. The correlation between Hg enrichments, tuffaceous layers, and recorded shift in
656 $^{187}\text{Os}/^{188}\text{Os}_{(i)}$ ratios to unradiogenic compositions further suggests that all three could have been caused
657 by the same volcanic process. Given that the volcanic activity that caused the shift in seawater Os-
658 isotope ratio represented a six- to tenfold increase on pre-event background activity (Bauer *et al.*, 2017),
659 it is highly unlikely that the volcanism responsible for the recorded Hg enrichment and $^{187}\text{Os}/^{188}\text{Os}_{(i)}$
660 shift at DSDP Site 463, which appears to have occurred at least proximally to the G-OJP, can have been

anything other than intense activity on that LIP. Moreover, given the intensity of this LIP volcanism, the fact that the mercury enrichment only appears in a site proximal to the G-OJP, and not correlative with $^{187}\text{Os}/^{188}\text{Os}_{(i)}$ shifts in the Tethyan realm, supports predominantly submarine eruptions, as also concluded by previous studies based on trends in other trace-element concentrations and lead-isotope signatures (Kuroda *et al.*, 2011; Erba *et al.*, 2015). The differing seawater residence times of osmium (10s kyr) and mercury (100s yr) would have enabled unradiogenic Os sourced from this volcanism to mix throughout the global ocean, whilst rapid Hg scavenging limited any evidence of a mercury flux to near the G-OJP, as documented in this study.

The slight possibility that the correlative Hg enrichment and $^{187}\text{Os}/^{188}\text{Os}_{(i)}$ shift at DSDP Site 463 were caused by HALIP volcanism is ruled out by the absence of a similar Hg peak in the C3 sediments of the Tethyan and (especially) DH-1 archives. It is possible that the one data-point Hg spike at the base of the C3 level in the DH-1 core represents a volcanic Hg flux from the HALIP that was then overprinted by excess TOC burial (as previously proposed for other sites by Percival *et al.*, 2015, and Charbonnier and Föllmi, 2017), but this interpretation is speculative, and there is also no evidence for such an overprinting of increased Hg concentrations at any other site (Figure 4 and Supplementary Figure 1). If the HALIP had emitted sufficient mercury to the atmosphere to reach the Pacific, it is highly unlikely that there would be little clear record of such Hg output in any of the comparatively proximal Arctic or European/Tethyan sedimentary records (see Figure 2). Thus, the G-OJP is more likely to have been the primary source of mercury to the Mid-Pacific Mountains (and unradiogenic osmium to the global ocean as a whole).

Despite an apparent lack of impact on the Hg cycle, it cannot be excluded that the HALIP (as well as other carbon sources such as methane clathrates; e.g., Jahren *et al.*, 2001) still contributed to causing the global C-cycle perturbation associated with OAE 1a. Such a scenario would likely have relied upon HALIP magmatic sills intruding organic-rich sediments with a low Hg content, causing massive emissions of isotopically light carbon, but little mercury output. However, it is not currently known whether such lithologies exist around the HALIP sills. Moreover, this scenario is at odds with

the documentation of Hg-cycle perturbations in stratigraphic records of several events linked with LIPs thought to have featured thermogenic volatile emissions (e.g., Percival *et al.*, 2015, 2017; Jones *et al.*, 2019; Shen *et al.*, 2019b), and with preliminary investigations of carbon and mercury contents in shales intruded by LIP magmas in South Africa, which show clear evidence for remobilisation of both volatiles (Svensen *et al.*, 2018). Therefore, it is more likely that the role played by the HALIP in initiating OAE 1a (if any) was minor compared to that of G-OJP activity.

5.3 Volcanic vs terrestrial sources of Hg to marine environments after the onset of OAE 1a

More plausibly, the widespread sedimentary Hg enrichments documented across C4 (or even the very uppermost C3) to C5 strata of seven out of nine OAE 1a sites studied here and by Charbonnier and Föllmi (2017) might have been triggered by a perturbation of the atmospheric mercury inventory following emissions of the element to the atmosphere from one or both of HALIP volcanism and sill intrusion of organic-rich shales. Given that subaerial LIP volcanism is thought to have emitted large volumes of Hg to the atmosphere at other times in Earth's history (e.g., Sanei *et al.*, 2012; Percival *et al.*, 2017, 2018; Grasby *et al.*, 2019), similar eruptions on areas of the G-OJP that emerged above the sea surface could also have produced this effect. However, because the C4–C5 strata postdate the onset of OAE 1a by on the order of 10s kyr (Li *et al.*, 2008; Malinverno *et al.*, 2010), the sedimentary Hg peaks might also result from lithological/redox changes or an increased input of terrigenous material following environmental responses to the climate disruption associated with the event.

As outlined in section 1.3, mercury can be deposited in sediments bound to sulphides, particularly in euxinic water columns (Shen *et al.*, 2020). In this context, the fact that the Cismon core records the development of euxinic conditions during OAE 1a (e.g., van Breugel *et al.*, 2007), and that C4 (and C6) strata from that archive marked by increased Hg concentrations also feature elevated sulphur contents (Supplementary Figure 2B), may indicate a switch to mercury burial with sulphides in the Belluno Basin during OAE 1a. If this association between Hg and S was the case, it could suggest

that redox changes and pyrite-deposition controlled sedimentary Hg contents at that location during OAE 1a, rather than any external influx. And if so, it is likely that a similar situation existed for the PLG core, given the similar palaeoenvironments and Hg/TOC records of the Cismon and PLG records (only one or two high data points that do not exceed pre-event levels, or at least their range of uncertainty). Whilst this local redox/sulphide control on mercury for these two sites remains unproven, the relative paucity of high Hg/TOC values nonetheless means that robust evidence of a consistent external flux of mercury to the Belluno and Umbria-Marche basins during OAE 1a is currently lacking.

However, C4–C5 strata, specifically, of Notre-Dame-de-Rosans, La Bédoule, Glaise, and DSDP Site 463 record no evidence of euxinic conditions under which deposition of mercury with sulphides would have been most likely (Mélières *et al.*, 1981; van Breugel *et al.*, 2007; Westermann *et al.*, 2013; Giraud *et al.*, 2018), although DSDP Site 463 does feature an increased pyrite abundance in the C4 segment (Mélières *et al.*, 1981). Euxinic conditions are extremely unlikely to have developed in the nearshore shallow-marine environment recorded by the DH-1 core, and a reasonably oxic (or at least not severely anoxic) setting is supported for that record by low sedimentary molybdenum and uranium concentrations, which show little or no enrichment above average-shale values except for two samples above the Selli Level Equivalent (*this study*; see Supplementary Figure 2C). There is also no correlation between the C4–C5 Hg enrichments and abundance of clays/Al₂O₃ at any of DSDP Site 463, the DH-1 core, La Bédoule, or Glaise (see Supplementary Figure 2, and Charbonnier and Föllmi, 2017). These trends support a lack of association between mercury and clay minerals in the C4–C5 strata at those sites, which would be expected due to the abundant TOC content in these same sediments, given the likely greater affiliation for mercury with organic matter over clays when both phases are present (Shen *et al.*, 2020). Thus, for at least four or five locations spanning the Arctic, Pacific, and north-western Tethyan realms presented here and in Charbonnier and Föllmi (2017), there is no evidence that mercury was deposited with a phase other than organic matter, making it likely that the C4–C5 peaks in Hg and Hg/TOC values were caused by an increased influx of mercury rather than lithological/redox changes.

Charcoal particles potentially indicative of wildfire activity have been reported from strata of Aptian age (Brown *et al.*, 2012; Wang *et al.*, 2019), although not from the Selli Level Equivalent specifically, or in any of the nine sites studied here and by Charbonnier and Föllmi (2017). Thus, there is no positive evidence that the widespread Hg influxes were the result of wildfires, although such a source cannot be completely ruled out. Nonetheless, terrestrially derived organic matter is abundant in the DH-1 core, and is thought to be present in some mixture with marine material at all of DSDP Site 463, Notre-Dame-de-Rosans, and Glaise (van Breugel *et al.*, 2007; Westermann *et al.*, 2013; Midtkandal *et al.* 2016; Giraud *et al.*, 2018). Organic-matter contents are too low at La Bédoule to reliably determine their composition. Thus, an increased input of terrigenous organic matter during a time of increased riverine runoff is a theoretically plausible source of the mercury to these sites during the early–middle part of OAE 1a, as previously proposed for the Early Jurassic Toarcian OAE (Them *et al.*, 2019). However, peak weathering rates during OAE 1a are thought to have been during C3 rather than C4 (Tejada *et al.*, 2009; Bottini *et al.*, 2012; Lechler *et al.*, 2015). Thus, if the mercury were derived from runoff of terrestrial material, an enrichment would be expected in the C3 segment rather than C4–C5 strata. Moreover, there is no evidence for an enhanced flux of mercury to the depositional setting of the Petrobras Well D core, despite an increase in the content of terrestrially derived organic matter in the upper part of the OAE 1a level (Tedeschi *et al.*, 2020).

Consequently, whilst local terrestrial runoff cannot be discounted as the cause of the widespread C4–C5 Hg-cycle perturbations, LIP-related emissions of mercury to the atmosphere provide an equally plausible explanation. In the latter scenario, overprinting of Hg by excess TOC might have muted any record of Hg/TOC peaks at sites such as Cismon or PLG (see Charbonnier and Föllmi, 2017). As noted above, the lack of clear evidence of volcanic activity in the northwest Tethys during latest Barremian to early Aptian times means that local eruptions cannot be unambiguously stated as the cause of the observed C4–C5 Hg enrichments in Tethyan stratigraphic archives. Future studies incorporating mercury-isotope analyses may aid determination of the pathways taken by the element to reach depositional environments, and potentially indicate whether LIP activity or local processes such as

terrestrial runoff and/or wildfires were the main cause of the widespread Hg enrichments recorded in the C4–C5 segments (c.f., Grasby *et al.*, 2017; Them *et al.*, 2019).

5.4 Implications for the impact of magmatic CO₂ emissions from LIPs on the global carbon cycle

Even if the widespread Hg-cycle disturbances during the early–middle (C4–C5) part of OAE 1a were related to subaerial volcanism and/or HALIP-related thermogenic volatile emissions, this activity apparently did not commence until after the onset of the event. Thus, it is unlikely that these processes played a major role in triggering the crisis. Instead, the combined Hg enrichments at DSDP Site 463 and lack of clear C3 peaks from elsewhere strongly support submarine volcanism on the G-OJP as the dominant form of LIP activity during the onset of OAE 1a, suggesting magmatic CO₂ output from that province as the main driver of the carbon-cycle perturbations that initiated climate change. Such a scenario supports the model of Bauer *et al.* (2017) that G-OJP mantle-carbon emissions were sufficient to cause the pronounced negative CIE documented in C3 strata that record the onset of OAE 1a.

However, it remains unclear whether G-OJP volcanism caused a global carbon-cycle perturbation simply due to the huge volume ($59\text{--}77\times 10^6\text{ km}^3$; Kerr and Mahoney, 2007), and high basaltic emplacement rate (possibly $>100\text{ km}^3/\text{yr}$; see introduction) of that LIP, particularly if it was combined with activity on the previously postulated twin province emplaced onto the Farallon Plate (Schlanger *et al.*, 1981; Larson, 1991). If carbon emissions associated with the uniquely voluminous/rapid G-OJP magmatism were solely responsible for the negative CIE at the onset of OAE 1a, it would not detract from previous hypotheses that most (smaller) LIPs do not emit sufficient magmatic CO₂ to drive such disturbances unless combined with thermogenic volatiles and/or methane hydrate release (e.g., Hesselbo *et al.*, 2000; Self *et al.*, 2006). However, these results might also

highlight the possibility that all LIPs can drive such disturbances through magmatic carbon emissions alone (as previously hypothesized by e.g., Saunders, 2016; Gutjahr *et al.*, 2017). Further studies of (intrusive and extrusive) LIP basalts and sediments intruded by magmatic sills, both for the G-OJP, HALIP and other provinces, are needed in order to constrain the potential outputs of different volatile species from magmatic and thermogenic sources, and to determine the extent to which these different sources could have perturbed the cycling of different elements at the Earth's surface during different geological periods.

6. CONCLUSIONS

This study has investigated the influence of different magmatic processes related to the development of large igneous provinces (LIPs) on the global environment, using OAE 1a as a case study. By combining new mercury data for six records of that event, including the first sites studied outside of the Tethyan realm, and new osmium-isotope evidence from one of these six (Poggio le Guaine) with previously published datasets, the types of LIP activity likely to have been most prevalent during the onset and main body of the event have been determined.

Although osmium-isotope trends are broadly consistent across all new and previously studied sites in documenting intense LIP activity throughout OAE 1a, records of mercury-cycle disturbance show considerable geographical variability. The only unambiguous Hg perturbation during the onset of OAE 1a (matching Os-isotope evidence of LIP activity) is recorded in the Mid-Pacific Mountains very proximal to the Greater Ontong-Java Plateau (G-OJP). No such clear evidence for mercury-cycle perturbations at that time is recorded at Tethyan or South Atlantic sites, or from the Arctic region proximal to the High Arctic Large Igneous Province (HALIP). This pattern supports G-OJP volcanism as the dominant form of LIP activity at the onset of OAE 1a, causing the globally documented Os-isotope shift but only localized Hg enrichment. These findings also re-emphasise previous hypotheses that oceanic LIPs only influence mercury cycling in immediately proximal regions, due to the limited

dispersal range of Hg emitted by submarine volcanism and other subaqueous basalt–seawater interactions, and likely do not cause a global-scale perturbation.

Crucially, whilst submarine LIP activity on the G-OJP during the onset of OAE 1a is clearly documented by osmium-isotope and mercury evidence, there is no clear indication for HALIP magmatism at that time. More widespread, if generally less pronounced, mercury-cycle perturbations appear to have taken place during the early–middle (C4–C5) part of OAE 1a. These disturbances could have been linked to a transient pulse in subaerial eruptions or thermogenic emissions related to the emplacement of the HALIP, or an intensification of/switch to subaerial eruptions on the G-OJP. However, a non-volcanic cause of these widespread Hg-cycle disturbances after the onset of OAE 1a, resulting from local environmental degradation during the event, cannot be ruled out. Even if these widespread mercury enrichments do signify sub-aerial LIP activity, the observation that they are not recorded globally in sediments that mark the onset of OAE 1a strongly suggests that such processes could not have caused the event. Instead, the results appear to confirm that submarine volcanism active on the Greater Ontong-Java Plateau, rather than sill intrusions of organic-rich sediments by the High Arctic LIP, was likely the primary trigger for OAE 1a.

ACKNOWLEDGEMENTS

We greatly appreciate feedback from two anonymous reviewers that has improved this manuscript. We gratefully acknowledge John Farmer and the University of Edinburgh for provision of geochemical standard material, Stéphane Reboulet for fieldwork assistance at the Notre-Dame-de-Rosans section, and Steve Wyatt for aiding laboratory analyses. The Poggio le Guaine (PLG) core drilling was financially supported by the Fundação de Apoio à Universidade de São Paulo and Petrobras grant 2405. Peter Szatmari is thanked for conducting the logistical arrangements required to perform rhenium-osmium analyses on PLG samples at the University of Alberta. The UNIS CO2 Lab is thanked for providing access to the DH-1 core samples, and we greatly appreciate assistance from Sverre Planke, Ivar Midtkandal, and Stéphane Polteau in sampling the core. We thank the UK

Natural Environment Research Council (NERC) grant NE/G01700X/1 (to Tamsin Mather), the European Research Council consolidator grant ERC-2018-COG-B18717-V-ECHO (to Tamsin Mather), NERC PhD studentship NE/L501530/1 (to Lawrence Percival), the Flanders Research Foundation (FWO) grant no. 12P4519N (to Lawrence Percival), the MIURPRIN (Ministero dell'Istruzione, dell'Università e della Ricerca-Progetti di Ricerca di Interesse Nazionale: grant no. PRIN 2017RX9XXXY to Elisabetta Erba), the Research Council of Norway Centres of Excellence (Project 223272 to Henrik Svensen), Petrobras (for financial support of the PLG and Petrobras Well D analyses and doctoral student funding for Leonardo R. Tedeschi), the Vrije Universiteit Brussel, and the Leverhulme Trust for funding.

REFERENCES

- Adloff, M., Greene, S.E., Parkinson, I.J., Naafs, B.D.A., Preston, W., Ridgwell, A., Lunt, D.J., Castro, J.M. and Monteiro, F.M., 2020, Unravelling the sources of carbon emissions at the onset of Oceanic Anoxic Event (OAE) 1a. *Earth and Planetary Science Letters*, 530, 115947, <https://doi.org/10.1016/j.epsl.2019.115947>.
- Allègre, C.J., Birck, J.L., Capmas, F. and Courtillot, V., 1999, Age of the Deccan traps using ^{187}Re – ^{187}Os systematics. *Earth and Planetary Science Letters*, 170, p. 197–204, [https://doi.org/10.1016/S0012-821X\(99\)00110-7](https://doi.org/10.1016/S0012-821X(99)00110-7).
- Ando, A., Kaiho, K., Kawahata, H. and Kakegawa, T., 2008, Timing and magnitude of early Aptian extreme warming: Unraveling primary $\delta^{18}\text{O}$ variation in indurated pelagic carbonates at Deep Sea Drilling Project Site 463, central Pacific Ocean. *Palaeogeography, Palaeoclimatology, Palaeoecology*, 260, p. 463–476, <https://doi.org/10.1016/j.palaeo.2007.12.007>.
- Ando, A., 2015, Intersite discrepancy in the amplitude of marine negative $\delta^{13}\text{C}$ excursion at the onset of early Aptian oceanic anoxic event 1a: Reconciliation through Sr isotopic screening of peculiar diagenetic overprint on the Pacific reference section (Deep Sea Drilling Project Site 463). In Neal, C.R., Sager, W.W., Sano, T. and Erba, E. (Eds.), *The Origin, Evolution, and Environmental Impact of Oceanic*

Large Igneous Provinces, Geological Society of America Special Paper, 511, p. 329–339,
[https://doi.org/10.1130/2015.2511\(17\)](https://doi.org/10.1130/2015.2511(17)).

Ando, T., Sawada, K., Takashima, R. and Nishi, H., 2013, Paleoproductivity of dinoflagellate and cyanobacteria during the mid-Cretaceous oceanic anoxic events in the Vocontian Basin, SE France. 26th IMOG Organic Geochemistry: Trends for the 21st Century, 2, p. 330–331.

Bagnato, E., Aiuppa, A., Parello, F., Calabrese, S., D'Alessandro, W., Mather, T.A., McGonigle, A.J.S., Pyle, D.M. and Wängberg, I., 2007, Degassing of gaseous (elemental and reactive) and particulate mercury from Mount Etna volcano (Southern Italy). *Atmospheric Environment*, 41, p.7377–7388,
<https://doi.org/10.1016/j.atmosenv.2007.05.060>.

Baudin, F., Fiet, N., Coccioni, R. and Galeotti, S., 1998, Organic matter characterisation of the Selli Level (Umbria-Marche Basin, central Italy). *Cretaceous Research*, 19, p. 701–714,
<https://doi.org/10.1006/cres.1998.0126>.

Bauer, K.W., Zeebe, R.E. and Wortmann, U.G., 2017, Quantifying the volcanic emissions which triggered Oceanic Anoxic Event 1a and their effect on ocean acidification. *Sedimentology*, 64, p. 204–214,
<https://doi.org/10.1111/sed.12335>.

Behar, F., Beaumont, V. and de B. Pentead, H.L., 2001, Rock-Eval 6 technology: performances and developments. *Oil & Gas Science and Technology*, 56, p. 111–134,
<https://doi.org/10.2516/ogst:2001013>.

Bond, D.P.G. and Wignall, P.B., 2014, Large igneous provinces and mass extinctions: an update. *In* Keller, G. and Kerr A.C. (Eds.), *Volcanism, Impacts, and Mass Extinctions: Causes and Effects*, Geological Society of America Special Papers, 505, SPE505-02, [https://doi.org/10.1130/2014.2505\(02\)](https://doi.org/10.1130/2014.2505(02)).

913 Bottini, C., Cohen, A.S., Erba, E., Jenkyns, H.C. and Coe, A.L., 2012, Osmium-isotope evidence for volcanism,
 914 weathering, and ocean mixing during the early Aptian OAE 1a. *Geology*, 40, p. 583–586,
 915 <https://doi.org/10.1130/G33140.1>.
 916

917 Bottini, C., Erba, E., Tiraboschi, D., Jenkyns, H.C., Schouten, S. and Sinninghe Damsté, J.S., 2015, Climate
 918 variability and ocean fertility during the Aptian Stage. *Climate of the Past*, 11, p. 383–402,
 919 <https://doi.org/10.5194/cp-11-383-2015>.
 920

921 Bowman, K.L., Hammerschmidt, C.R., Lamborg, C.H. and Swarr, G., 2015, Mercury in the North Atlantic Ocean:
 922 The U.S. GEOTRACERS zonal and meridional sections. *Deep-Sea Research II*, 116, p. 251–261,
 923 <https://doi.org/10.1016/j.dsr2.2014.07.004>.
 924

925 Bralower, T.J., Arthur, M.A., Leckie, R.M., Sliter, W.V., Allard, D.J. and Schlanger, S.O., 1994, Timing and
 926 paleoceanography of oceanic dysoxia/anoxia in the Late Barremian to Early Aptian (Early
 927 Cretaceous). *Palaios*, p. 335–369, <https://doi.org/10.2307/3515055>.
 928

929 Bréhéret, J.G., 1997, L'Aptien et l'Albien de la fosse vocontienne (des bordures au bassin): Evolution de la
 930 sédimentation et enseignements sur les événements anoxiques. *Société Géologique du Nord Publication*
 931 25, 614 p.
 932

933 Bréhéret, J.G., 1998, Episodes de sédimentation riche en matière organique dans les marnes bleues d'âge aptien
 934 et albien de la partie pélagique du bassin vocontien. *Bulletin de la Société géologique de France*, 4, p.
 935 349–356, <https://doi.org/10.2113/gssgfbull.IV.2.349>.
 936

937 Brown, S.A.E., Scott, A.C., Glasspool, I.J. and Collinson, M.E., 2012, Cretaceous wildfires and their impact on
 938 the Earth system. *Cretaceous research*, 36, p. 162–190, <https://doi.org/10.1016/j.cretres.2012.02.008>.
 939

940 Caillaud, A., Quijada, M., Huet, B., Reynaud, J.Y., Riboulleau, A., Bout-Roumazielles, V., Baudin, F., Chappaz,
 941 A., Adatte, T., Ferry, J.N. and Tribovillard, N., 2020, Turbidite-induced re-oxygenation episodes of the

sediment-water interface in a diverticulum of the Tethys Ocean during the Oceanic Anoxic Event 1a:
The French Vocontian Basin. *The Depositional Record*, 6, p. 352–382, <https://doi.org/10.1002/dep2.102>.

Chaboureaud, A.C., Guillocheau, F., Robin, C., Rohais, S., Moulin, M. and Aslanian, D., 2013, Paleogeographic
evolution of the central segment of the South Atlantic during Early Cretaceous times: Paleotopographic
and geodynamic implications. *Tectonophysics*, 604, p. 191–223,
<https://doi.org/10.1016/j.tecto.2012.08.025>.

Chambers, L.M., Pringle, M.S. and Fitton, J.G., 2004, Phreatomagmatic eruptions on the Ontong Java Plateau: an
Aptian $^{40}\text{Ar}/^{39}\text{Ar}$ age for volcanoclastic rocks at ODP Site 1184. *In* Fitton, J.G., Mahoney, J.J., Wallace,
P.J. and Saunders, A.D. (Eds.), *Origin and Evolution of the Ontong Java Plateau*, Geological Society of
London, Special Publications, 229, p. 325–331, <https://doi.org/10.1144/GSL.SP.2004.229.01.18>.

Channell, J.E.T., Erba, E., Muttoni, G. and Tremolada, F., 2000, Early Cretaceous magnetic stratigraphy in the
APTICORE drill core and adjacent outcrop at Cison (Southern Alps, Italy), and correlation to the
proposed Barremian-Aptian boundary stratotype. *Geological Society of America Bulletin*, 112, p. 1430–
1443, [https://doi.org/10.1130/0016-7606\(2000\)112<1430:ECMSIT>2.0.CO;2](https://doi.org/10.1130/0016-7606(2000)112<1430:ECMSIT>2.0.CO;2).

Charbonnier, G. and Föllmi, K.B., 2017, Mercury enrichments in lower Aptian sediments support the link between
Ontong Java large igneous province activity and oceanic anoxic episode 1a. *Geology*, 45, p. 63–66,
<https://doi.org/10.1130/G38207.1>.

Charbonnier, G., Morales, C., Duchamp-Alphonse, S., Westermann, S., Adatte, T. and Föllmi, K.B., 2017,
Mercury enrichment indicates volcanic triggering of Valanginian environmental change. *Scientific
reports*, 7, <https://doi.org/10.1038/srep40808>.

Charbonnier, G., Adatte, T., Spangenberg, J.E. and Föllmi, K.B., 2018a, The expression of early Aptian to latest
Cenomanian oceanic anoxic events in the sedimentary record of the Briançonnais domain. *Global and
planetary change*, 170, p. 76–92, <https://doi.org/10.1016/j.gloplacha.2018.08.009>.

Charbonnier, G., Godet, A., Bodin, S., Adatte, T. and Föllmi, K.B., 2018b, Mercury anomalies, volcanic pulses, and drowning episodes along the northern Tethyan margin during the latest Hauterivian-earliest Aptian. *Palaeogeography, Palaeoclimatology, Palaeoecology*, 505, p. 337–350, <https://doi.org/10.1016/j.palaeo.2018.06.013>.

Charbonnier, G., Adatte, T., Föllmi, K.B. and Suan, G., 2020, Effect of intense weathering and post-depositional degradation of organic matter on Hg/TOC proxy in organic-rich sediments and its implications for deep-time investigations. *Geochemistry, Geophysics, Geosystems*, 21, <https://doi.org/10.1029/2019GC008707>.

Coccioni, R., Nesci, O., Tramontana, M., Wezel, F.C. and Moretti, E., 1987, Descrizione di un livello-guida "radiolaritico-bituminoso-ittiolitico" alla base delle Marne a Furoidi nell'Appennino umbro-marchigiano. *Bollettino della Società Geologica Italiana*, 106, p. 183–192.

Coccioni, R., Franchi, R., Nesci, O., Perilli, N., Wezel, F.C. and Battistini, F., 1990, Stratigrafia, micropaleontologia e mineralogia delle Marne a Furoidi delle sezioni di Poggio le Guaine e del Fiume Bosso (Appennino umbro-marchigiano). *Atti 2° Convegno Internazionale "Fossili, Evoluzione, Ambiente"*, Pergola, 25-30 ottobre 1987. Tecnostampa, p. 163–201.

Coccioni, R., Jovane, L., Bancalà, G., Bucci, C., Fauth, G., Frontalini, F., Janikian, L., Savian, J., Paes de Almeida, R., Mathias, G.L. and Ferreira da Trindade, I.R., 2012, Umbria-Marche Basin, Central Italy: A reference section for the Aptian-Albian interval at low latitudes. *Scientific Drilling*, 13, p. 42–46, <https://doi.org/10.2204/iodp.sd.13.07.2011>.

Cogné, J.P. and Humler, E., 2006, Trends and rhythms in global seafloor generation rate. *Geochemistry, Geophysics, Geosystems*, 7, <https://doi.org/10.1029/2005GC001148>.

Cohen, A. S. and Coe, A. L., 2002, New geochemical evidence for the onset of volcanism in the Central Atlantic magmatic province and environmental change at the Triassic-Jurassic boundary. *Geology*, 30, p. 267–270, [https://doi.org/10.1130/0091-7613\(2002\)030<0267:NGEFTO>2.0.CO;2](https://doi.org/10.1130/0091-7613(2002)030<0267:NGEFTO>2.0.CO;2).

1002

1003 Cohen, A.S., Coe, A.L., Bartlett, J.M. and Hawkesworth, C.J., 1999, Precise Re-Os ages of organic-rich mudrocks
1004 and the Os isotope composition of Jurassic seawater. *Earth and Planetary Science Letters*, 167, p. 159–
1005 173, [https://doi.org/10.1016/S0012-821X\(99\)00026-6](https://doi.org/10.1016/S0012-821X(99)00026-6).

1006

1007 Corfu, F., Polteau, S., Planke, S., Faleide, J.I., Svensen, H., Zayoncheck, A. and Stolbov, N., 2013, U–Pb
1008 geochronology of Cretaceous magmatism on Svalbard and Franz Josef Land, Barents Sea large igneous
1009 province. *Geological Magazine*, 150, p. 1127–1135, <https://doi.org/10.1017/S0016756813000162>.

1010

1011 Cumming, V.M., Poulton, S.W., Rooney, A.D. and Selby, D., 2013, Anoxia in the terrestrial environment during
1012 the late Mesoproterozoic. *Geology*, 41, p. 583–586, <https://doi.org/10.1130/G34299.1>.

1013

1014 Daga, R., Guevara, S.R., Pavlin, M., Rizzo, A., Lojen, S., Vreča, P., Horvat, M. and Arribére, M., 2016, Historical
1015 records of mercury in southern latitudes over 1600 years: Lake Futalaufquen, Northern
1016 Patagonia. *Science of the Total Environment*, 553, p. 541–550,
1017 <https://doi.org/10.1016/j.scitotenv.2016.02.114>.

1018

1019 Dean, W.E., Claypool, G.E. and Thide, J., 1984, Accumulation of organic matter in Cretaceous oxygen-
1020 deficient depositional environments in the central Pacific Ocean. *Organic geochemistry*, 7, p. 39–51,
1021 [https://doi.org/10.1016/0146-6380\(84\)90135-9](https://doi.org/10.1016/0146-6380(84)90135-9).

1022

1023 Dickson, A.J., Cohen, A.S., Coe, A.L., Davies, M., Shcherbinina, E.A. and Gavrillov, Y.O., 2015, Evidence for
1024 weathering and volcanism during the PETM from Arctic and Peri-Tethys osmium isotope records.
1025 *Palaeogeography, Palaeoclimatology, Palaeoecology*, 438, p. 300–307,
1026 <https://doi.org/10.1016/j.palaeo.2015.08.019>.

1027

1028 Dockman, D.M., Pearson, D.G., Heaman, L.M., Gibson, S.A. and Sarkar, C., 2018, Timing and origin of
1029 magmatism in the Sverdrup Basin, Northern Canada—Implications for lithospheric evolution in the High
1030 Arctic Large Igneous Province (HALIP). *Tectonophysics*, 742, p. 50–65,
1031 <https://doi.org/10.1016/j.tecto.2018.05.010>.

1032
1033
1034
1035
1036
1037
1038
1039
1040
1041
1042
1043
1044
1045
1046
1047
1048
1049
1050
1051
1052
1053
1054
1055
1056
1057
1058
1059
1060
1061

Dumitrescu M. and Brassell S.C., 2006, Compositional and isotopic characteristics of organic matter for the early Aptian Oceanic Anoxic Event at Shatsky Rise, ODP Leg 198. *Palaeogeography, Palaeoclimatology, Palaeoecology*, 235, p. 168–191, <https://doi.org/10.1016/j.palaeo.2005.09.028>.

Erba, E., 1994, Nannofossils and superplumes: the early Aptian “nannoconid crisis”. *Paleoceanography and Paleoclimatology*, 9, p. 483–501, <https://doi.org/10.1029/94PA00258>.

Erba, E., 2004, Calcareous nannofossils and Mesozoic oceanic anoxic events. *Marine micropaleontology*, 52, p. 85–106, <https://doi.org/10.1016/j.marmicro.2004.04.007>.

Erba, E. and Larson, R.L., 1998, The Cismon APTICORE (Southern Alps, Italy): a "reference section" for the Lower Cretaceous at low latitudes. *Rivista Italiana di Paleontologia e Stratigrafia (Research In Paleontology and Stratigraphy)*, 104, p. 181–192.

Erba, E. and Tremolada, F., 2004, Nannofossil carbonate fluxes during the Early Cretaceous: Phytoplankton response to nutrification episodes, atmospheric CO₂, and anoxia. *Paleoceanography*, 19, <https://doi.org/10.1029/2003PA000884>.

Erba, E., Channell, J.E.T., Claps, M., Jones, C., Larson, R., Opdyke, B., Premoli Silva, I., Riva, A., Salvini, G. and Torricelli, S., 1999, Integrated stratigraphy of the Cismon Apticore (southern Alps, Italy); a "reference section" for the Barremian-Aptian interval at low latitudes. *Journal of Foraminiferal Research*, 29, p. 371–391.

Erba, E., Bottini, C., Weissert, H.J. and Keller, C.E., 2010, Calcareous nannoplankton response to surface-water acidification around Oceanic Anoxic Event 1a. *Science*, 329, p. 428–432, <https://doi.org/10.1126/science.1188886>.

Erba, E., Duncan, R.A., Bottini, C., Tiraboschi, D., Weissert, H., Jenkyns, H.C. and Malinverno, A., 2015, Environmental consequences of Ontong Java Plateau and Kerguelen Plateau volcanism. *In* Neal, C.R.,

1062 Sager, W.W., Sano, T. and Erba, E. (Eds.), The Origin, Evolution, and Environmental Impact of Oceanic
 1063 Large Igneous Provinces, Geological Society of America Special Paper, 511, p. 271–303,
 1064 [https://doi.org/10.1130/2015.2511\(15\)](https://doi.org/10.1130/2015.2511(15)).
 1065
 1066 Ericksen, J.A., Gustin, M.S., Schorran, D.E., Johnson, D.W., Lindberg, S.E. and Coleman, J.S., 2003,
 1067 Accumulation of atmospheric mercury in forest foliage. *Atmospheric Environment*, 36,
 1068 p. 1613–1622, [https://doi.org/10.1016/S1352-2310\(03\)00008-6](https://doi.org/10.1016/S1352-2310(03)00008-6).
 1069
 1070 Finlay, A.J., Selby, D. and Gröcke, D.R., 2010, Tracking the Hirnantian glaciation using Os isotopes. *Earth and*
 1071 *Planetary Science Letters*, 293, p. 339–348, <https://doi.org/10.1016/j.epsl.2010.02.049>.
 1072
 1073 Föllmi, K.B., Godet, A., Bodin, S. and Linder, P., 2006, Interactions between environmental change and shallow
 1074 water carbonate buildup along the northern Tethyan margin and their impact on the Early Cretaceous
 1075 carbon isotope record. *Paleoceanography*, 21, <https://doi.org/10.1029/2006PA001313>.
 1076
 1077 Gales, E., Black, B. and Elkins-Tanton, L.T., 2020, Carbonatites as a record of the carbon isotope composition of
 1078 large igneous province outgassing. *Earth and Planetary Science Letters*, 535, 116076,
 1079 <https://doi.org/10.1016/j.epsl.2020.116076>.
 1080
 1081 Giraud, F., Pittet, B., Grosheny, D., Baudin, F., Lécuyer, C. and Sakamoto, T., 2018, The palaeoceanographic
 1082 crisis of the Early Aptian (OAE 1a) in the Vocontian Basin (SE France). *Palaeogeography*,
 1083 *Palaeoclimatology*, *Palaeoecology*, 511, p. 483–505, <https://doi.org/10.1016/j.palaeo.2018.09.014>.
 1084
 1085 Gladczenko, T.P., Coffin, M.F. and Eldholm, O., 1997, Crustal structure of the Ontong Java Plateau: modeling of
 1086 new gravity and existing seismic data. *Journal of Geophysical Research: Solid Earth*, 102, p. 22711–
 1087 22729, <https://doi.org/10.1029/97JB01636>.
 1088
 1089 Grasby, S.E., Beauchamp, B., Bond, D.P.G., Wignall, P.B. and Sanei, H., 2016, Mercury anomalies associated
 1090 with three extinction events (Capitanian crisis, latest Permian extinction and the Smithian/Spathian

1091 extinction) in NW Pangea. Geological Magazine, 153, p. 285–297,
 1092 <https://doi.org/10.1017/S0016756815000436>.
 1093
 1094 Grasby, S.E., Wenjie, S., Runsheng, Y., Gleason, J.D., Blum, J.D., Lepak, R.F., Hurley, J.P. and Beauchamp, B.,
 1095 2017, Isotopic signatures of mercury contamination in latest Permian oceans. *Geology*, 45, p. 55–58,
 1096 <https://doi.org/10.1130/G38487.1>.
 1097
 1098 Grasby, S.E., Them, T.R., Chen, Z., Yin, R. and Ardakani, O.H., 2019, Mercury as a proxy for volcanic emissions
 1099 in the geologic record. *Earth-Science Reviews*, 196, 102880
 1100 <https://doi.org/10.1016/j.earscirev.2019.102880>.
 1101
 1102 Gröcke, D.R., Hesselbo, S.P. and Jenkyns, H.C., 1999, Carbon-isotope composition of Lower Cretaceous fossil
 1103 wood: Ocean-atmosphere chemistry and relation to sea-level change. *Geology*, 27, p. 155–158,
 1104 [https://doi.org/10.1130/0091-7613\(1999\)027<0155:CICOLC>2.3.CO;2](https://doi.org/10.1130/0091-7613(1999)027<0155:CICOLC>2.3.CO;2).
 1105
 1106 Gutjahr, M., Ridgwell, A., Sexton, P.F., Anagnostou, E., Pearson, P.N., Pälike, H., Norris, R.D., Thomas, E. and
 1107 Foster, G.L., 2017, Very large release of mostly volcanic carbon during the Palaeocene–Eocene Thermal
 1108 Maximum. *Nature*, 548, p. 573–577, <https://doi.org/10.1038/nature23646>.
 1109
 1110 Hammer, Ø., Jones, M.T., Schneebeili-Hermann, E., Hansen, B.B. and Bucher, H., 2019, Are Early Triassic
 1111 extinction events associated with mercury anomalies? A reassessment of the Smithian/Spathian boundary
 1112 extinction. *Earth-Science Reviews*, 195, p. 179–190, <https://doi.org/10.1016/j.earscirev.2019.04.016>.
 1113
 1114 Hein, J.R. and Vanek, E., 1981, Origin and alteration of volcanic ash and pelagic brown clay, Deep Sea Drilling
 1115 Project Leg 62, north-central Pacific. Initial Reports of the Deep Sea Drilling Project, 62, p. 559–569
 1116 <https://doi.org/10.2973/dsdp.proc.62.120.1981>.
 1117
 1118 Hesselbo, S.P., Gröcke, D.R., Jenkyns, H.C., Bjerrum, C.J., Farrimond, P., Morgans-Bell, H.S. and Green, O.R.,
 1119 2000, Massive dissociation of gas hydrate during a Jurassic oceanic anoxic event. *Nature*, 406, p. 392–
 1120 395, <https://doi.org/10.1038/35019044>.

1121

1122 Hibsich, C., Jandel, D., Montenat, C. and Ott d'Estevou, P., 1992, Evénements tectoniques crétacés dans la partie
 1123 méridionale du bassin subalpin (massif Ventoux-Lure et partie orientale de l'arc de Castellane, SE
 1124 France). Implications géodynamiques. Bulletin de la Société Géologique de France, 163, p. 147–158.

1125

1126 Hoernle, K., Hauff, F., van den Bogaard, P., Werner, R., Mortimer, N., Geldmacher, J., Garbe-Schönberg, D. and
 1127 Davy, B., 2010, Age and geochemistry of volcanic rocks from the Hikurangi and Manihiki oceanic
 1128 Plateaus. *Geochimica et Cosmochimica Acta*, 74, p. 7196–7219,
 1129 <https://doi.org/10.1016/j.gca.2010.09.030>.

1130

1131 Hönsch, B., Ridgwell, A., Schmidt, D.N., Thomas, E., Gibbs, S.J., Sluijs, A., Zeebe, R., Kump, L., Martindale,
 1132 R.C., Greene, S.E., Kiessling, W., Ries, J., Zachos, J.C., Royer, D.L., Barker, S., Marchitto, T.M., Moyer,
 1133 R., Pelejero, C., Ziveri, P., Foster, G.L. and Williams, B., 2012, The geological record of ocean
 1134 acidification. *Science*, 335, p. 1058–1063, <https://doi.org/10.1126/science.1208277>.

1135

1136 Hu, X., Zhao, K., Yilmaz, I.O. and Li, Y., 2012, Stratigraphic transition and palaeoenvironmental changes from
 1137 the Aptian oceanic anoxic event 1a (OAE 1a) to the oceanic red bed 1 (ORB1) in the Yenicesihlar section,
 1138 central Turkey. *Cretaceous Research*, 38, p. 40–51, <https://doi.org/10.1016/j.cretres.2012.01.007>.

1139

1140 Jähren, A.H., Arens, N.C., Sarmiento, G., Guerrero, J. and Amundson, R., 2001, Terrestrial record of methane
 1141 hydrate dissociation in the Early Cretaceous. *Geology*, 29, p. 159–162, [https://doi.org/10.1130/0091-](https://doi.org/10.1130/0091-7613(2001)029<0159:TROMHD>2.0.CO;2)
 1142 [7613\(2001\)029<0159:TROMHD>2.0.CO;2](https://doi.org/10.1130/0091-7613(2001)029<0159:TROMHD>2.0.CO;2).

1143

1144 Jenkyns, H.C., 1988, The early Toarcian (Jurassic) anoxic event: Stratigraphic, sedimentary, and geochemical
 1145 evidence. *American Journal of Science*, 288, p. 101–151, <https://doi.org/10.2475/ajs.288.2.101>.

1146

1147 Jenkyns, H.C., 1995, Carbon-isotope stratigraphy and paleoceanographic significance of the Lower Cretaceous
 1148 shallow-water carbonates of Resolution Guyot, Mid-Pacific Mountains. *In* Winterer, E.L., Sager, W.W.,
 1149 Firth, J.V. and Sinton J.M. (Eds.), *Proceedings of the Ocean Drilling Program, Scientific Results*, 143,

1150 p. 99–104. College Station, Texas, Ocean Drilling Program,
 1151 <https://doi.org/10.2973/odp.proc.sr.143.213.1995>.
 1152
 1153 Jenkyns, H.C., 2010, Geochemistry of oceanic anoxic events. *Geochemistry, Geophysics, Geosystems*, 11,
 1154 <https://doi.org/10.1029/2009GC002788>.
 1155
 1156 Jenkyns, H.C., 2018, Transient cooling episodes during Cretaceous Oceanic Anoxic Events with special reference
 1157 to OAE 1a (Early Aptian). *Philosophical Transactions of the Royal Society A: Mathematical, Physical*
 1158 *and Engineering Sciences*, 376, 20170073, <https://doi.org/10.1098/rsta.2017.0073>.
 1159
 1160 Jones, C.E. and Jenkyns, H.C., 2001, Seawater strontium isotopes, oceanic anoxic events, and seafloor
 1161 hydrothermal activity in the Jurassic and Cretaceous. *American Journal of Science*, 301, p. 112–149,
 1162 <https://doi.org/10.2475/ajs.301.2.112>.
 1163
 1164 Jones, M.T., Percival, L.M.E., Stokke, E.W., Frieling, J., Mather, T.A., Riber, L., Schubert, B.A., Schultz, B.,
 1165 Tegner, C., Planke, S. and Svensen H., 2019, Mercury anomalies across the Palaeocene–Eocene Thermal
 1166 Maximum. *Climate of the Past*, 15, p. 217–236, <https://doi.org/10.5194/cp-15-217-2019>.
 1167
 1168 Kendall, B., Creaser, R.A., Reinhard, C.T., Lyons, T.W. and Anbar, A.D., 2015, Transient episodes of mild
 1169 environmental oxygenation and oxidative continental weathering during the late Archean. *Science*
 1170 *Advances*, 1, e1500777, <https://doi.org/10.1126/sciadv.1500777>.
 1171
 1172 Kerr, A.C. and Mahoney, J.J., 2007, Oceanic plateaus: Problematic plumes, potential paradigms. *Chemical*
 1173 *Geology*, 241, p. 332–353, <https://doi.org/10.1016/j.chemgeo.2007.01.019>.
 1174
 1175 Kongchum, M., Hudnall, W.H. and Delaune, R.D., 2011, Relationship between sediment clay minerals and total
 1176 mercury. *Journal of Environmental Science and Health, Part A*, 46, p. 534–539,
 1177 <https://doi.org/10.1080/10934529.2011.551745>.
 1178

- Koutsoukos, E.A.M., 1992, Late Aptian to Maastrichtian foraminiferal biogeography and palaeoceanography of the Sergipe Basin, Brazil. *Palaeogeography, palaeoclimatology, palaeoecology*, 92, p. 295–324, [https://doi.org/10.1016/0031-0182\(92\)90089-N](https://doi.org/10.1016/0031-0182(92)90089-N).
- Kuhnt, W., Holbourn, A. and Moullade, M., 2011, Transient global cooling at the onset of early Aptian oceanic anoxic event (OAE) 1a. *Geology*, 39, p. 323–326, <https://doi.org/10.1130/G31554.1>.
- Kuroda, J., Tanimizu, M., Hori, R.S., Suzuki, K., Ogawa, N.O., Tejada, M.L.G., Coffin, M.F., Coccioni, R., Erba, E. and Ohkouchi, N., 2011, Lead isotopic record of Barremian–Aptian marine sediments: Implications for large igneous provinces and the Aptian climatic crisis. *Earth and Planetary Science Letters*, 307, p. 126–134, <https://doi.org/10.1016/j.epsl.2011.04.021>.
- Larson, R.L., 1991, Latest pulse of Earth: Evidence for a mid-Cretaceous superplume. *Geology*, 19, p. 547–550, [https://doi.org/10.1130/0091-7613\(1991\)019<0547:LPOEEF>2.3.CO;2](https://doi.org/10.1130/0091-7613(1991)019<0547:LPOEEF>2.3.CO;2).
- Larson, R.L. and Erba, E., 1999, Onset of the Mid-Cretaceous greenhouse in the Barremian-Aptian: Igneous events and the biological, sedimentary, and geochemical responses. *Paleoceanography*, 14, <https://doi.org/10.1029/1999PA900040>.
- Lechler, M., Pogge von Strandmann, P.A.E., Jenkyns, H.C., Prosser, G. and Parente, M., 2015, Lithium-isotope evidence for enhanced silicate weathering during OAE 1a (Early Aptian Selli event). *Earth and Planetary Science Letters*, 432, p. 210–222, <https://doi.org/10.1016/j.epsl.2015.09.052>.
- Li, Y.X., Bralower, T.J., Montañez, I.P., Osleger, D.A., Arthur, M.A., Bice, D.M., Herbert, T.D., Erba, E. and Silva, I.P., 2008, Toward an orbital chronology for the early Aptian Oceanic Anoxic Event (OAE1a, ~120 Ma). *Earth and Planetary Science Letters*, 271, p. 88–100, <https://doi.org/10.1016/j.epsl.2008.03.055>.

1207 Lowrie, W., Alvarez, W., Silva, I.P. and Monechi, S., 1980, Lower Cretaceous magnetic stratigraphy in Umbrian
 1208 pelagic carbonate rocks. *Geophysical Journal International*, 60, p. 263–281,
 1209 <https://doi.org/10.1111/j.1365-246X.1980.tb04292.x>.
 1210
 1211 Malinverno, A., Erba, E. and Herbert, T.D., 2010, Orbital tuning as an inverse problem: Chronology of the early
 1212 Aptian oceanic anoxic event 1a (Selli Level) in the Cismon APTICORE. *Paleoceanography and*
 1213 *Paleoclimatology*, 25, <https://doi.org/10.1029/2009PA001769>.
 1214
 1215 McElwain, J.C., Wade-Murphy, J. and Hesselbo, S.P., 2005, Changes in carbon dioxide during an oceanic anoxic
 1216 event linked to intrusion into Gondwana coals. *Nature*, 435, p. 479–482,
 1217 <https://doi.org/10.1038/nature03618>.
 1218
 1219 Méhay, S., Keller, C.E., Bernasconi, S.M., Weissert, H., Erba, E., Bottini, C. and Hochuli, P.A., 2009, A volcanic
 1220 CO₂ pulse triggered the Cretaceous Oceanic Anoxic Event 1a and a biocalcification crisis. *Geology*, 37,
 1221 p. 819–822, <https://doi.org/10.1130/G30100A.1>.
 1222
 1223 Mélières, F., Deroo, G. and Herbin, J.P., 1981, Organic-matter-rich and hypersiliceous Aptian sediments from
 1224 western Mid-Pacific Mountains. *Initial Reports of the Deep Sea Drilling Project*, 62, p. 903–915,
 1225 <https://doi.org/10.2973/dsdp.proc.62.146.1981>.
 1226
 1227 Menegatti, A.P., Weissert, H., Brown, R.S., Tyson, R.V., Farrimond, P., Strasser, A. and Caron, M., 1998, High-
 1228 resolution $\delta^{13}\text{C}$ stratigraphy through the early Aptian “Livello Selli” of the Alpine
 1229 Tethys. *Paleoceanography*, 13, <https://doi.org/10.1029/98PA01793>.
 1230
 1231 Midtkandal, I., Svensen, H., Planke, S., Corfu, F., Polteau, S., Torsvik, T.H., Faleide, J.I., Grundvåg, S.A., Selnes,
 1232 H., Kürschner, W. and Olaussen, S., 2016, The Aptian (Early Cretaceous) oceanic anoxic event (OAE1a)
 1233 in Svalbard, Barents Sea, and the absolute age of the Barremian-Aptian boundary. *Palaeogeography,*
 1234 *Palaeoclimatology, Palaeoecology*, 463, p. 126–135, <https://doi.org/10.1016/j.palaeo.2016.09.023>.
 1235

1236 Mutterlose, J., Bottini, C., Schouten, S. and Sinninghe Damsté, J.S., 2014, High sea-surface temperatures during
 1237 the early Aptian Oceanic Anoxic Event 1a in the Boreal Realm. *Geology*, 42, p. 439–442,
 1238 <https://doi.org/10.1130/G35394.1>.
 1239
 1240 Naafs, B.D.A. and Pancost, R.D., 2016, Sea-surface temperature evolution across Aptian Oceanic Anoxic Event
 1241 1a. *Geology*, 44, p. 959–962, <https://doi.org/10.1130/G38575.1>.
 1242
 1243 Naafs, B.D.A., Castro, J.M., De Gea, G.A., Quijano, M.L., Schmidt, D.N. and Pancost, R.D., 2016, Gradual and
 1244 sustained carbon dioxide release during Aptian Oceanic Anoxic Event 1a. *Nature Geoscience*, 9, p. 135–
 1245 139, <https://doi.org/10.1038/ngeo2627>.
 1246
 1247 Neumann, E.R., Svensen, H., Tegner, C., Planke, S., Thirlwall, M. and Jarvis, K.E., 2013, Sill and lava
 1248 geochemistry of the mid-Norway and NE Greenland conjugate margins. *Geochemistry, Geophysics,*
 1249 *Geosystems*, 14, <https://doi.org/10.1002/ggge.20224>.
 1250
 1251 Pancost, R.D., Crawford, N., Magness, S., Turner, A., Jenkyns, H.C. and Maxwell, J.R., 2004, Further evidence
 1252 for the development of photic-zone euxinic conditions during Mesozoic oceanic anoxic events. *Journal*
 1253 *of the Geological Society*, 161, p. 353–364, <https://doi.org/10.1144/0016764903-059>.
 1254
 1255 Paquay, F.S. and Ravizza, G., 2012, Heterogeneous seawater $^{187}\text{Os}/^{188}\text{Os}$ during the late Pleistocene
 1256 glaciations. *Earth and Planetary Science Letters*, 349, p. 126–138,
 1257 <https://doi.org/10.1016/j.epsl.2012.06.051>.
 1258
 1259 Percival, L.M.E., Witt, M.L.I., Mather, T.A., Hermoso, M., Jenkyns, H.C., Hesselbo, S.P., Al-Suwaidi, A.H.,
 1260 Storm, M.S., Xu, W. and Ruhl, M., 2015, Globally enhanced mercury deposition during the end-
 1261 Pliensbachian extinction and Toarcian OAE: A link to the Karoo–Ferrar Large Igneous Province. *Earth*
 1262 *and Planetary Science Letters*, 428, p. 267–280, <https://doi.org/10.1016/j.epsl.2015.06.064>.
 1263
 1264 Percival, L.M.E., Ruhl, M., Hesselbo, S.P., Jenkyns, H.C., Mather, T.M. and Whiteside, J.H., 2017, Mercury
 1265 evidence for pulsed volcanism during the end-Triassic mass extinction. *Proceedings of the National*

1266 Academy of Sciences of the United States of America, 114, p. 7929–7934,
 1267 <https://doi.org/10.1073/pnas.1705378114>.
 1268

1269 Percival, L.M.E., Jenkyns, H.C., Mather, T.A., Dickson, A.J., Batenburg, S.J., Ruhl, M., Hesselbo, S.P., Barclay,
 1270 R., Jarvis, I., Robinson, S.A., Woelders, L., 2018, Does Large Igneous Province volcanism always
 1271 perturb the mercury cycle? Comparing the records of Oceanic Anoxic Event 2 and the end-Cretaceous
 1272 to other Mesozoic events. *American Journal of Science*, 318 p. 799–860,
 1273 <https://doi.org/10.2475/08.2018.01>.
 1274

1275 Percival, L.M.E., Bergquist, B.A., Mather, T.A. and Sanei, H., 2021, Sedimentary mercury enrichments as a tracer
 1276 of Large Igneous Province volcanism. In Ernst, R.E., Dickson, A.J., Bekker, A. (Eds.): *Large Igneous*
 1277 *Provinces: A Driver of Global Environmental and Biotic Change*. AGU Geophysical Monograph, 255,
 1278 p. 247–262, <https://doi.org/10.1002/9781119507444.ch11>.
 1279

1280 Peucker-Ehrenbrink, B. and Jahn, B.M., 2001, Rhenium-osmium isotope systematics and platinum group element
 1281 concentrations: Loess and the upper continental crust. *Geochemistry, Geophysics, Geosystems*, 2,
 1282 <https://doi.org/10.1029/2001GC000172>.
 1283

1284 Peucker-Ehrenbrink, B. and Ravizza, G., 2000, The marine osmium isotope record. *Terra Nova*, 12, p. 205–219,
 1285 <https://doi.org/10.1046/j.1365-3121.2000.00295.x>.
 1286

1287 Polteau, S., Hendriks, B.W.H., Planke, S., Ganerød, M., Corfu, F., Faleide, J.I., Midtkandal, I., Svensen, H. and
 1288 Kylebust, R., 2016, The Early Cretaceous Barents Sea Sill Complex: Distribution, $^{40}\text{Ar}/^{39}\text{Ar}$
 1289 geochronology, and implications for carbon gas formation. *Palaeogeography, Palaeoclimatology,*
 1290 *Palaeoecology*, 441, p. 83–95, <https://doi.org/10.1016/j.palaeo.2015.07.007>.
 1291

1292 Price, G.D., 2003, New constraints upon isotope variation during the early Cretaceous (Barremian–Cenomanian)
 1293 from the Pacific Ocean. *Geological Magazine*, 140, p. 513–522,
 1294 <https://doi.org/10.1017/S0016756803008100>.
 1295

1296 Pyle, D.M., and Mather, T.A., 2003, The importance of volcanic emissions for the global atmospheric mercury
1297 cycle. *Atmospheric Environment*, 37, p. 5115–5124, <https://doi.org/10.1016/j.atmosenv.2003.07.011>.
1298

1299 Robinson, S.A., Clarke, L.J., Nederbragt, A. and Wood, I.G., 2008, Mid-Cretaceous oceanic anoxic events in the
1300 Pacific Ocean revealed by carbon-isotope stratigraphy of the Calera Limestone, California,
1301 USA. *Geological Society of America Bulletin*, 120, p. 1416–1426, <https://doi.org/10.1130/B26350.1>.
1302

1303 Robinson, S.A., Heimhofer, U., Hesselbo, S.P. and Petrizzo, M.R., 2017, Mesozoic climates and oceans – a tribute
1304 to Hugh Jenkyns and Helmut Weissert. *Sedimentology*, 64, p. 1–15, <https://doi.org/10.1111/sed.12349>.
1305

1306 Sanei, H., Grasby, S.E. and Beauchamp, B., 2012, Latest Permian mercury anomalies. *Geology*, 40, p. 63–66,
1307 <https://doi.org/10.1130/G32596.1>.
1308

1309 Saunders, A.D., 2016, Two LIPs and two Earth-system crises: the impact of the North Atlantic Igneous Province
1310 and the Siberian Traps on the Earth-surface carbon cycle. *Geological Magazine*, 153, p. 201–222,
1311 <https://doi.org/10.1017/S0016756815000175>.
1312

1313 Savian, J., Trindade, R., Janikian, L., Jovane, L., de Almeida, R.P., Coccioni, R., Frontalini, F., Sideri, M.,
1314 Figueiredo, M., Tedeschi, L.R. and Jenkyns, H.C., 2016, The Barremian-Aptian boundary in the Poggio
1315 le Guaine core (central Italy): Evidence for magnetic polarity Chron M0r and oceanic anoxic event 1a.
1316 *In* Menichetti, M., Coccioni, R. and Montanari, A. (Eds.), *The Stratigraphic Record of Gubbio: Integrated*
1317 *Stratigraphy of the Late Cretaceous–Paleogene Umbria-Marche Pelagic Basin*, Geological Society of
1318 America Special Paper, 524, p. 57–78, [https://doi.org/10.1130/2016.2524\(05\)](https://doi.org/10.1130/2016.2524(05)).
1319

1320 Scaife, J.D., Ruhl, M., Dickson, A.J., Mather, T.A., Jenkyns, H.C., Percival, L.M.E., Hesselbo, S.P., Cartwright,
1321 J., Eldrett, J.S., Bergman, S.C. and Minisini, D., 2017, Sedimentary Mercury Enrichments as a Marker
1322 for Submarine Large Igneous Province Volcanism? Evidence from the Mid-Cenomanian Event and
1323 Oceanic Anoxic Event 2 (Late Cretaceous). *Geochemistry, Geophysics, Geosystems*, 18,
1324 <https://doi.org/10.1002/2017GC007153>.
1325

1326 Schoene, B., Eddy, M.P., Samperton, K.M., Keller, C.B., Keller, G., Adatte, T. and Khadri, S.F.R., 2019. U-Pb
 1327 constraints on pulsed eruption of the Deccan Traps across the end-Cretaceous mass
 1328 extinction. *Science*, 363, p. 862–866, <https://doi.org/10.1126/science.aau2422>.
 1329

1330 Schroeder, W.H. and Munthe J., 1998, Atmospheric mercury - An overview. *Atmospheric Environment*, 32, p.
 1331 809–822, [https://doi.org/10.1016/S1352-2310\(97\)00293-8](https://doi.org/10.1016/S1352-2310(97)00293-8).
 1332

1333 Schlanger, S.O. and Jenkyns, H.C., 1976, Cretaceous oceanic anoxic events: causes and consequences. *Geologie*
 1334 *en Mijnbouw*, 55, p. 179–184.
 1335

1336 Schlanger, S.O., Jenkyns, H.C. and Premoli-Silva, I., 1981, Volcanism and vertical tectonics in the Pacific Basin
 1337 related to global Cretaceous transgressions. *Earth and Planetary Science Letters*, 52, p. 435–449,
 1338 [https://doi.org/10.1016/0012-821X\(81\)90196-5](https://doi.org/10.1016/0012-821X(81)90196-5).
 1339

1340 Selby, D., 2007, Direct Rhenium-Osmium age of the Oxfordian-Kimmeridgian boundary, Staffin bay, Isle of
 1341 Skye, UK, and the Late Jurassic time scale. *Norwegian Journal of Geology*, 87, p. 291–299.
 1342

1343 Selby, D. and Creaser, R.A., 2003, Re–Os geochronology of organic rich sediments: an evaluation of organic
 1344 matter analysis methods. *Chemical Geology*, 200, p. 225–240, [https://doi.org/10.1016/S0009-](https://doi.org/10.1016/S0009-2541(03)00199-2)
 1345 [2541\(03\)00199-2](https://doi.org/10.1016/S0009-2541(03)00199-2).
 1346

1347 Self, S., Widdowson, M., Thordarson, T. and Jay, A.E., 2006, Volatile fluxes during flood basalt eruptions and
 1348 potential effects on the global environment: A Deccan perspective. *Earth and Planetary Science*
 1349 *Letters*, 248, p. 518–532, <https://doi.org/10.1016/j.epsl.2006.05.041>.
 1350

1351 Selin, N.E., 2009, Global Biogeochemical Cycling of Mercury: A Review. *Annual Review of Environment and*
 1352 *Resources*, 34, p. 43–63, <https://doi.org/10.1146/annurev.environ.051308.084314>.
 1353

1354 Shen, J., Algeo, T.J., Chen, J., Planavsky, N.J., Feng, Q., Yu, J. and Liu, J., 2019a, Mercury in marine
 1355 Ordovician/Silurian boundary sections of South China is sulfide-hosted and non-volcanic in origin. *Earth
 1356 and Planetary Science Letters*, 511, p. 130–140, <https://doi.org/10.1016/j.epsl.2019.01.028>.
 1357
 1358 Shen, J., Chen, J., Algeo, T.J., Yuan, S., Feng, Q., Yu, J., Zhou, L., O'Connell, B., Planavsky, N.J., 2019b,
 1359 Evidence for a prolonged Permian–Triassic extinction interval from global marine mercury records.
 1360 *Nature Communications*, 10, <https://doi.org/10.1038/s41467-019-09620-0>.
 1361
 1362 Shen, J., Feng, Q., Algeo, T.J., Liu, J., Zhou, C., Wei, W., Liu, J., Them II, T.R., Gill, B.C. and Chen, J., 2020,
 1363 Sedimentary host phases of mercury (Hg) and implications for use of Hg as a volcanic proxy. *Earth and
 1364 Planetary Science Letters*, 543, 116333, <https://doi.org/10.1016/j.epsl.2020.116333>.
 1365
 1366 Sliter, W.V., 1989, Aptian anoxia in the Pacific Basin. *Geology*, 17, p. 909–912, [https://doi.org/10.1130/0091-
 1367 7613\(1989\)017<0909:AAITPB>2.3.CO;2](https://doi.org/10.1130/0091-7613(1989)017<0909:AAITPB>2.3.CO;2).
 1368
 1369 Storm, M.S., Hesselbo, S.P., Jenkyns, H.C., Ruhl, M., Ullmann, C.V., Xu, W., Leng, M.J., Riding, J.B. and
 1370 Gorbanenko, O., 2020, Orbital pacing and secular evolution of the Early Jurassic carbon
 1371 cycle. *Proceedings of the National Academy of Sciences of the United States of America*, 117, p. 3974–
 1372 3982, <https://doi.org/10.1073/pnas.1912094117>.
 1373
 1374 Svensen, H., Planke, S., Malthé-Sørenssen, A., Jamtveit, B., Myklebust, R., Eidem, T.R. and Rey, S.S., 2004,
 1375 Release of methane from a volcanic basin as a mechanism for initial Eocene global warming. *Nature*,
 1376 429, p. 542–545, <https://doi.org/10.1038/nature02566>.
 1377
 1378 Svensen, H., Percival, L.M.E., Jones, M.T. and Mather, T.A., 2018, Release of mercury from black shale during
 1379 contact metamorphism and the implications for mercury as a volcanic proxy. *Geophysical Research
 1380 Abstracts*, 20, EGU2018-10291-1, EGU General Assembly.
 1381
 1382 Tarduno, J.A., Sliter, W.V., Bralower, T.J., McWilliams, M., Premoli-Silva, I. and Ogg, J.G., 1989, M-sequence
 1383 reversals recorded in DSDP sediment cores from the western Mid-Pacific Mountains and Magellan

1384 Rise. Geological Society of America Bulletin, 101, p. 1306–1316, <https://doi.org/10.1130/0016->
1385 7606(1989)101<1306:MSRRID>2.3.CO;2.

1386

1387 Taylor, B., 2006, The single largest oceanic plateau: Ontong Java–Manihiki–Hikurangi. Earth and Planetary
1388 Science Letters, 241, p. 372–380, <https://doi.org/10.1016/j.epsl.2005.11.049>.

1389

1390 Tedeschi, L.R., Jenkyns, H.C., Robinson, S.A., Lana, C.C., Menezes Santos, M.R.F. and Tognoli, F.M., 2020,
1391 Aptian carbon-isotope record from the Sergipe-Alagoas Basin: New insights into oceanic anoxic event
1392 1a and the timing of seawater entry into the South Atlantic. Newsletters on Stratigraphy, 53, p. 333–364,
1393 <https://doi.org/10.1127/nos/2019/0529>.

1394

1395 Tegner, C., Storey, M., Holm, P.M., Thorarinsson, S.B., Zhao, X., Lo, C.H. and Knudsen, M.F., 2011, Magmatism
1396 and Eurekan deformation in the High Arctic Large Igneous Province: ^{40}Ar – ^{39}Ar age of Kap Washington
1397 Group volcanics. North Greenland. Earth and Planetary Science Letters, 303, p. 203–214,
1398 <https://doi.org/10.1016/j.epsl.2010.12.047>.

1399

1400 Tejada, M. L. G., Suzuki, K., Kuroda, J., Coccioni, R., Mahoney, J. J., Ohkouchi, N., Sakamoto, T. and Tatsumi,
1401 Y., 2009, Ontong Java Plateau eruption as a trigger for the early Aptian oceanic anoxic event. Geology,
1402 37, p. 855–858, <https://doi.org/10.1130/G25763A.1>.

1403

1404 Them, T.R., Jagoe, C.H., Caruthers, A.H., Gill, B.C., Grasby, S.E., Gröcke, D.R., Yin, R. and Owens, J.D., 2019,
1405 Terrestrial sources as the primary delivery mechanism of mercury to the oceans across the Toarcian
1406 Oceanic Anoxic Event (Early Jurassic). Earth and Planetary Science Letters, 507, p. 62–72,
1407 <https://doi.org/10.1016/j.epsl.2018.11.029>.

1408

1409 Thiede, J. *et al.*, 1981, Site 463: Western Mid-Pacific Mountains. Initial Reports of the Deep Sea Drilling
1410 Project, 62, p. 33–156, <https://doi.org/10.2973/dsdp.proc.62.102.1981>.

1411

- Thiede, J., Dean, W.E., and Claypool, G.E., 1982, Oxygen-deficient depositional paleoenvironments in the mid-Cretaceous tropical and sub-tropical central Pacific Ocean. *In* Schlanger, S.O., and Cita, M.B. (Eds.), *Nature and origin of Cretaceous carbon-rich facies*: London, Academic Press, p. 79–100.
- Thordarson, T., 2004, Accretionary-lapilli-bearing pyroclastic rocks at ODP Leg 192 Site 1184: a record of subaerial phreatomagmatic eruptions on the Ontong Java Plateau. *In* Fitton, J.G., Mahoney, J.J., Wallace, P.J. and Saunders, A.D. (Eds.), *Origin and Evolution of the Ontong Java Plateau*, Geological Society of London, Special Publications, 229, p. 275–306, <https://doi.org/10.1144/GSL.SP.2004.229.01.16>.
- Turgeon, S.C. and Creaser, R.A., 2008. Cretaceous oceanic anoxic event 2 triggered by a massive magmatic episode. *Nature*, 454, p. 323–326, <https://doi.org/10.1038/nature07076>.
- Vallier, T.L. and Jefferson, W.S., 1981, Volcanogenic Sediments from Hess Rise and the Mid-Pacific Mountains, Deep Sea Drilling Project Leg 62. *In* Thiede, J. and Vallier, T.L. *et al.*, *Initial Reports of the Deep Sea Drilling Project*, 62, p. 545–557, <https://doi.org/10.2973/dsdp.proc.62.119.1981>.
- van Acken, D., Thomson, D., Rainbird, R.H. and Creaser, R.A., 2013, Constraining the depositional history of the Neoproterozoic Shaler Supergroup, Amundsen Basin, NW Canada: Rhenium-osmium dating of black shales from the Wynniatt and Boot Inlet Formations. *Precambrian Research*, 236, p. 124–131, <https://doi.org/10.1016/j.precamres.2013.07.012>.
- van Breugel, Y., Schouten, S., Tsikos, H., Erba, E., Price, G.D. and Sinninghe Damsté, J.S., 2007, Synchronous negative carbon isotope shifts in marine and terrestrial biomarkers at the onset of the early Aptian oceanic anoxic event 1a: Evidence for the release of ¹³C-depleted carbon into the atmosphere. *Paleoceanography*, 22, <https://doi.org/10.1029/2006PA001341>.
- Vickers, M.L., Price, G.D., Jerrett, R.M. and Watkinson, M., 2016, Stratigraphic and geochemical expression of Barremian–Aptian global climate change in Arctic Svalbard. *Geosphere*, 12, p. 1594–1605, <https://doi.org/10.1130/GES01344.1>.

- Wang, S., Shao, L.Y., Yan, Z.M., Shi, M.J. and Zhang, Y.H., 2019, Characteristics of Early Cretaceous wildfires in peat-forming environment, NE China. *Journal of Palaeogeography*, 8, <https://doi.org/10.1186/s42501-019-0035-5>.
- Weissert, H., 1989, C-isotope stratigraphy, a monitor of paleoenvironmental change: a case study from the Early Cretaceous. *Surveys in Geophysics*, 10, p. 1–61, <https://doi.org/10.1007/BF01901664>.
- Westermann, S., Stein, M., Matera, V., Fiet, N., Fleitmann, D., Adatte, T. and Föllmi, K.B., 2013, Rapid changes in the redox conditions of the western Tethys Ocean during the early Aptian oceanic anoxic event. *Geochimica et Cosmochimica Acta*, 121, p. 467–486, <https://doi.org/10.1016/j.gca.2013.07.023>.

FIGURE CAPTIONS

Figure 1: Previously published trends across the Selli Level Equivalent of the Cismon core for **A)** carbon isotopes and **B)** osmium isotopes and osmium concentrations (data from Erba *et al.*, 1999; Bottini *et al.*, 2012). The grey shaded area indicates the stratigraphic extent of Selli Level Equivalent sediments deposited during OAE 1a; the dashed grey line the Barremian–Aptian boundary at the base of magnetozone M0 (Erba *et al.*, 1999; Channell *et al.*, 2000; Bottini *et al.*, 2012). The stratigraphic levels of both the decline and crisis of nannoconids (Erba *et al.*, 1999) are indicated by thin dashed black lines, and the $\delta^{13}\text{C}$ segments (from Menegatti *et al.*, 1998) by solid thin black lines. See methods section for details on the calculation of initial seawater Os-isotope ratios ($^{187}\text{Os}/^{188}\text{Os}_{(i)}$) and sedimentary osmium concentrations ($[\text{Os}_{(i)}]$). Lithology, biostratigraphy, magnetostratigraphy, and carbon-isotope segments are sourced as for Figure 4.

Figure 2: Palaeogeographic map of the Barremian–Aptian world (~120 Ma). The positions of the HALIP and G-OJP are indicated by dark red areas. Locations A–F mark sites of sedimentary records investigated for mercury in this study (black squares = mercury and osmium-isotope data presented; black circles = mercury data presented). Locations G–I (black triangles) indicate sites previously studied for mercury

by Charbonnier and Föllmi (2017). Global map is adapted from van Breugel *et al.* (2007), with the western Tethys inset adapted from Giraud *et al.* (2018).

Figure 3: Stratigraphic correlation of $\delta^{13}\text{C}$ ratios, and recorded $^{187}\text{Os}/^{188}\text{Os}_{(i)}$ and $[\text{Os}_{(i)}]$ values at 120 Ma for the Poggio le Guaine (PLG) core. Stratigraphic scale is in metres. $\delta^{13}\text{C}$ values, biostratigraphy, and carbon-isotope segments are sourced as for Figure 4; all osmium data are from this study. Grey shaded area indicates the stratigraphic extent of the Selli Level.

Figure 4: Geochemical data plots for $\delta^{13}\text{C}$, TOC, Hg contents, and Hg/TOC ratios for DSDP Site 463, the Cismon core, Poggio le Guaine (PLG) core, Notre-Dame-de-Rosans, the DH-1 core, and Petrobras Well D. Semi-transparent Hg/TOC data points indicate Hg/TOC ratios based on TOC contents <0.2 wt% (below the limit of reliability recommended by Grasby *et al.*, 2016). The ± 15 ppb range of Hg concentration uncertainty is indicated on each Hg data plot by a pale red field; the 0.1 wt% uncertainty on TOC measurements is not visible on this scale. The uncertainty range for each Hg/TOC value based on ± 15 ppb Hg and ± 0.1 wt% TOC is shown on each Hg/TOC plot by a pale red field. Grey shaded areas indicate the stratigraphic extent of the Selli Level (at PLG) or equivalent strata deposited during OAE 1a (all other sites), the grey dashed line the Barremian–Aptian boundary, and thin black dashed lines the recorded decline and crisis of nannoconids. All stratigraphic scales are in metres. All Hg and Hg/TOC data are new for this study. TOC data are sourced as follows: the DSDP Site 463, Poggio le Guaine core and Notre-Dame-de-Rosans from this study; the Cismon core from Bottini *et al.* (2012) and this study; the DH-1 core from Midtkandal *et al.* (2016); Petrobras Well D from Tedeschi *et al.* (2020). $\delta^{13}\text{C}$ data and information on lithology, biostratigraphy, magnetostratigraphy, and carbon-isotope segmentation are sourced as follows: DSDP Site 463 from Tarduno *et al.* (1989), Erba (1994), Bottini *et al.* (2012), and Ando *et al.* (2015); the Cismon core from Menegatti *et al.* (1998), Erba *et al.* (1999), Channell *et al.* (2000); the Poggio le Guaine core from Savian *et al.* (2016); Notre-Dame-de-Rosans from Giraud *et al.* (2018); DH-1 core from Midtkandal *et al.* (2016); Petrobras Well D from Tedeschi *et al.* (2020). Previously published TOC data for DSDP Site 463 and Notre-Dame-de-Rosans that were not used for normalisation of Hg are sourced from Bottini *et al.* (2012) and Giraud *et al.* (2018), respectively. The $\delta^{13}\text{C}$ and Hg data from DSDP Site 463 and the Cismon and DH-1 cores are presented alongside evidence for clay and pyrite/sulphur contents in Supplementary Figure 2.

Figure 5: Stratigraphic correlation of Hg/TOC ratios and $^{187}\text{Os}/^{188}\text{Os}_{(i)}$ trends from DSDP Site 463 and the Cismon and Poggio le Guaine (PLG) cores. Semi-transparent Hg/TOC data points indicate Hg/TOC ratios based on TOC contents <0.2 wt% (below the limit of reliability recommended by Grasby *et al.*, 2016). The uncertainty range for each Hg/TOC value based on ± 15 ppb Hg and ± 0.1 wt% TOC is shown by the pale red field. Published Os data from DSDP Site 463 and the Cismon core are from Bottini *et al.* (2012); Poggio le Guaine Os data and all Hg data are from this study. Grey shaded areas indicate the stratigraphic extent of the Selli Level or equivalent OAE 1a strata, the grey dashed line the Barremian–Aptian boundary, and thin black dashed lines the recorded decline and crisis of nannoconids. All stratigraphic scales are in metres. Information on lithology, $\delta^{13}\text{C}$ values, biostratigraphy, magnetostratigraphy, and carbon-isotope segments are sourced as for Figure 4.

Figure 6: Stratigraphic correlation of mercury concentrations, Hg/TOC ratios, and recorded $^{187}\text{Os}/^{188}\text{Os}_{(i)}$ and $[\text{Os}_{(i)}]$ values at 120 Ma for DSDP Site 463. Semi-transparent Hg/TOC data points indicate Hg/TOC ratios based on TOC contents <0.2 wt% (below the limit of reliability recommended by Grasby *et al.*, 2016). Yellow lines mark the stratigraphic positions of tuffaceous layers (Thiede *et al.*, 1981). The grey shaded area indicates the stratigraphic extent of Selli Level Equivalent sediments deposited during OAE 1a, the grey dashed line the Barremian–Aptian boundary, and thin black dashed lines the recorded decline and crisis of nannoconids. All stratigraphic scales are in metres. Information on lithology, $\delta^{13}\text{C}$ values, biostratigraphy, magnetostratigraphy, and carbon-isotope segments are sourced as for Figure 4. The uncertainty range for each Hg and Hg/TOC value based on ± 15 ppb Hg and ± 0.1 wt% TOC are shown by the pale red field on their respective data plots.

Figure 1

CISMON CORE (BELLUNO BASIN, ITALY)

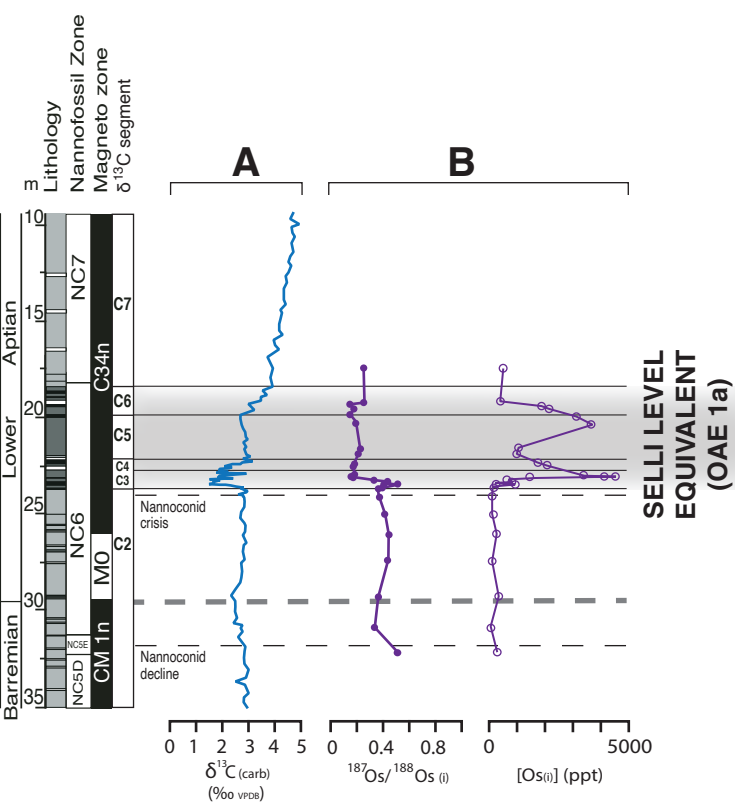


Figure 2

BARREMIAN–APTIAN PALAEOGEOGRAPHY (~120 Ma)

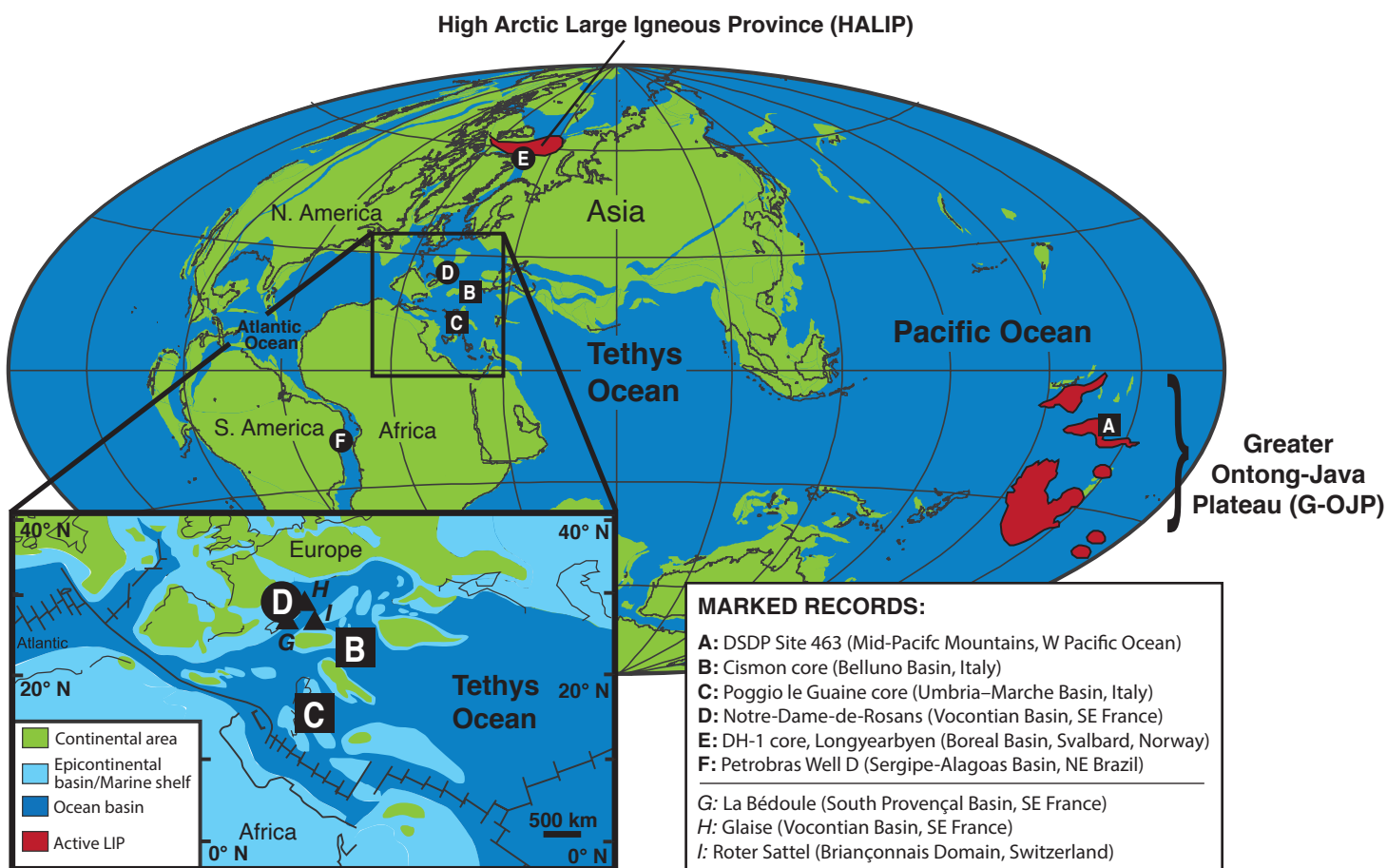


Figure 3

POGGIO LE GUAINA CORE
(UMBRIA-MARCHE BASIN, ITALY)

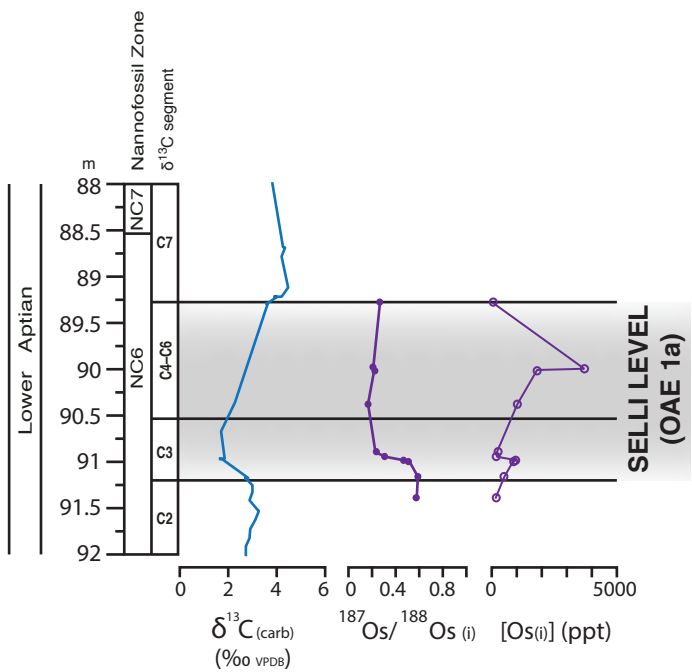
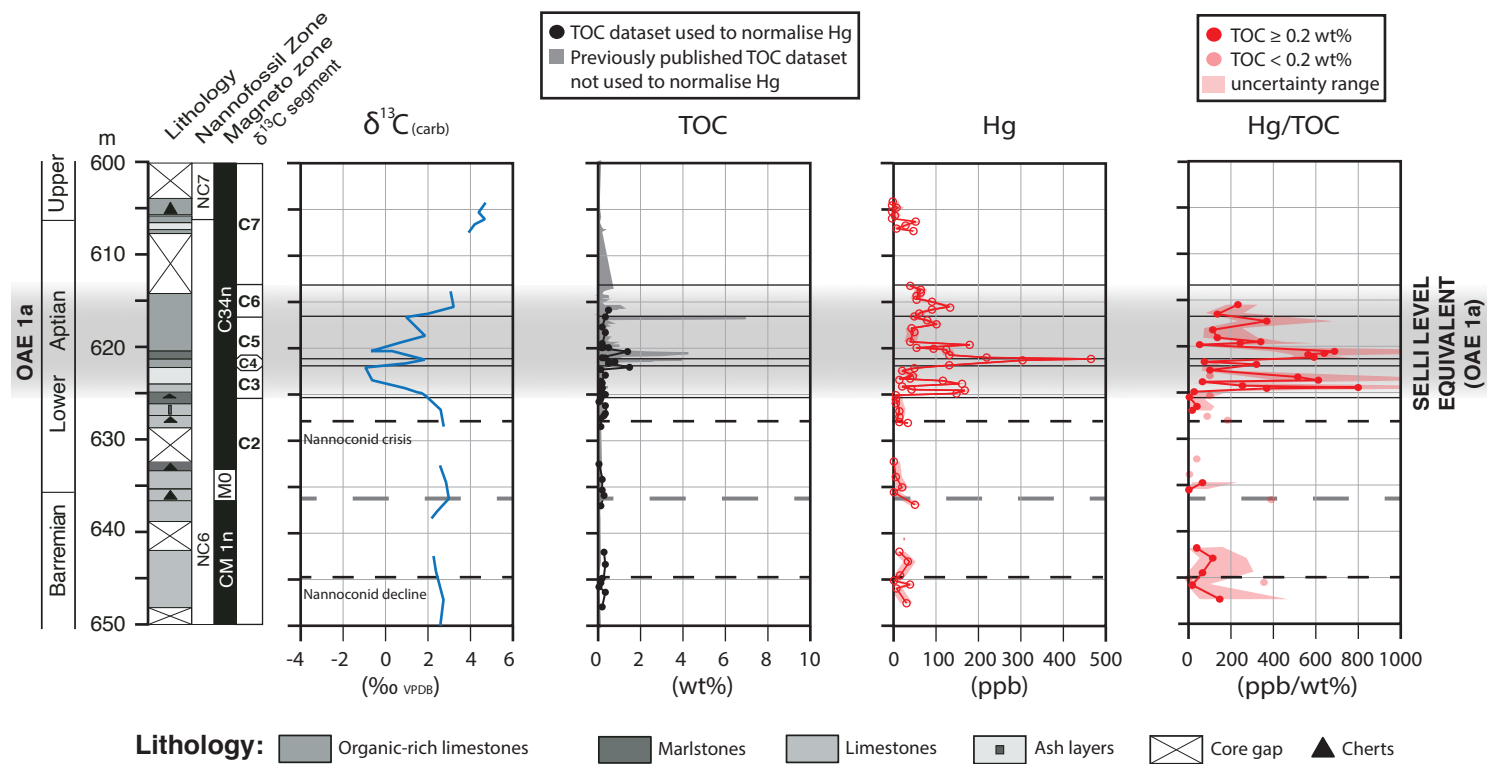


Figure 4

A: DSDP SITE 463 (MID-PACIFIC MOUNTAINS, W PACIFIC OCEAN)



B: CISMON CORE (BELLUNO BASIN, ITALY)

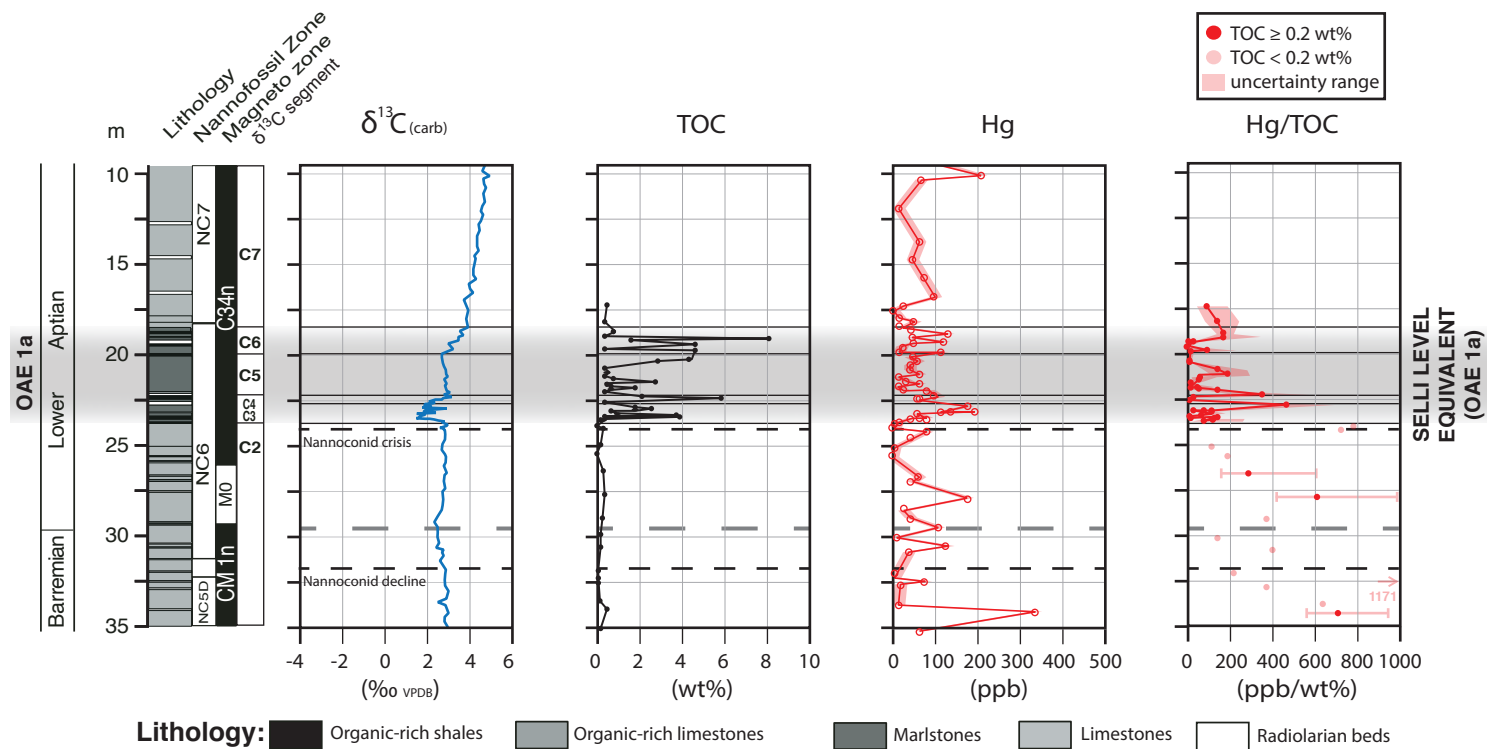
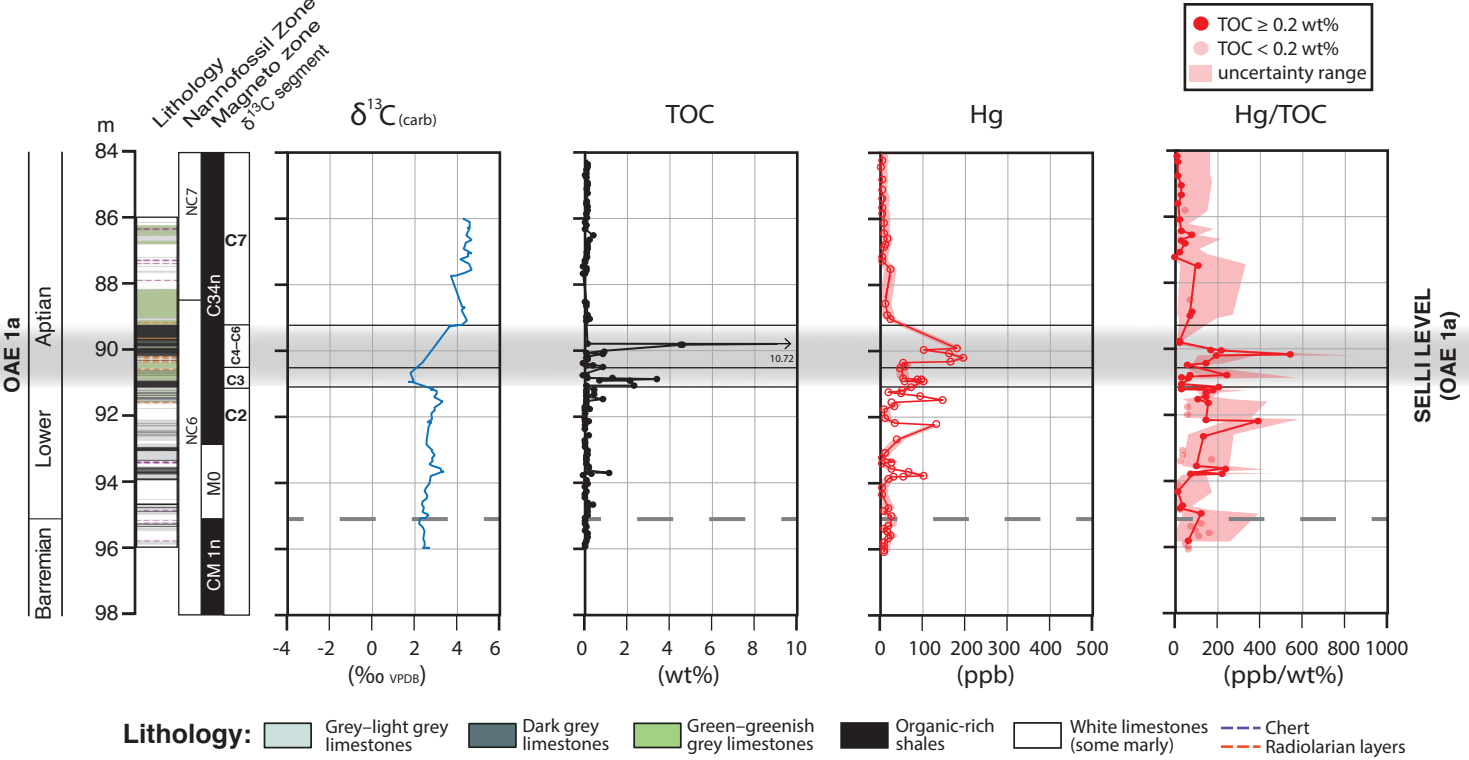


Figure 4

C: POGGIO LE GUAINES CORE (UMBRIA-MARCHE BASIN, ITALY)



D: NOTRE-DAME-DE-ROSANS (VOCONTIAN BASIN, SE FRANCE)

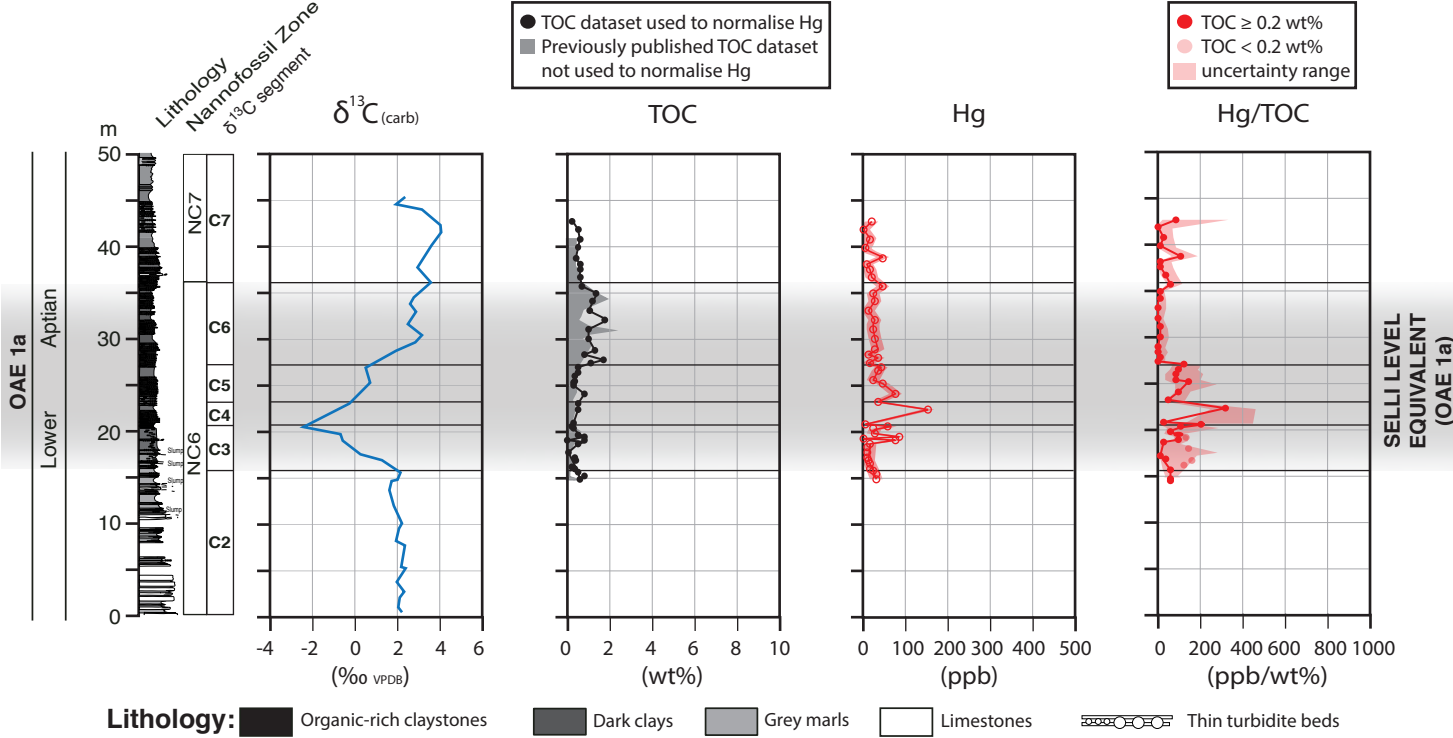
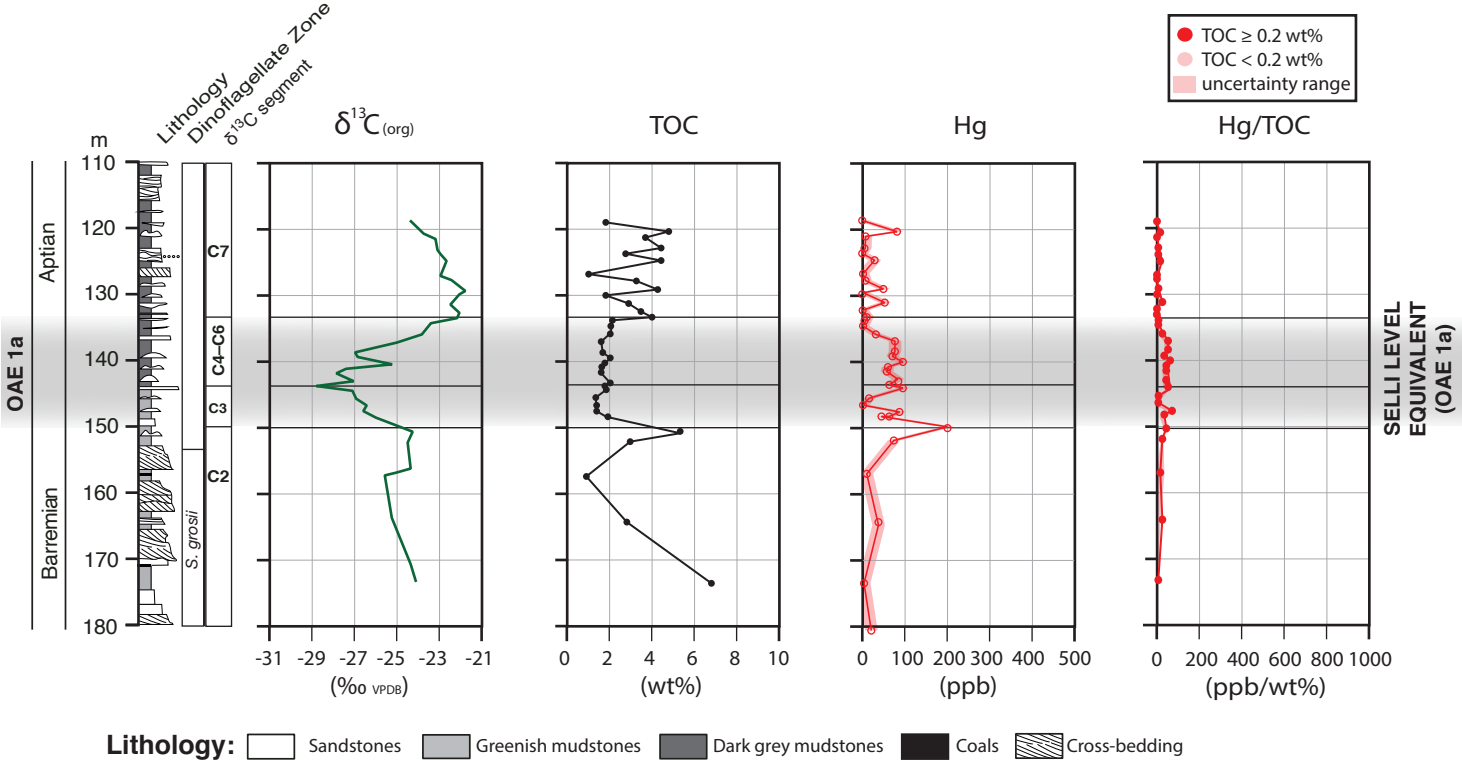


Figure 4

E: DH-1 CORE, LONGYEARBYEN (BOREAL BASIN, SVALBARD, NORWAY)



F: PETROBRAS WELL D (SERGIPE-ALAGOAS BASIN, NE BRAZIL)

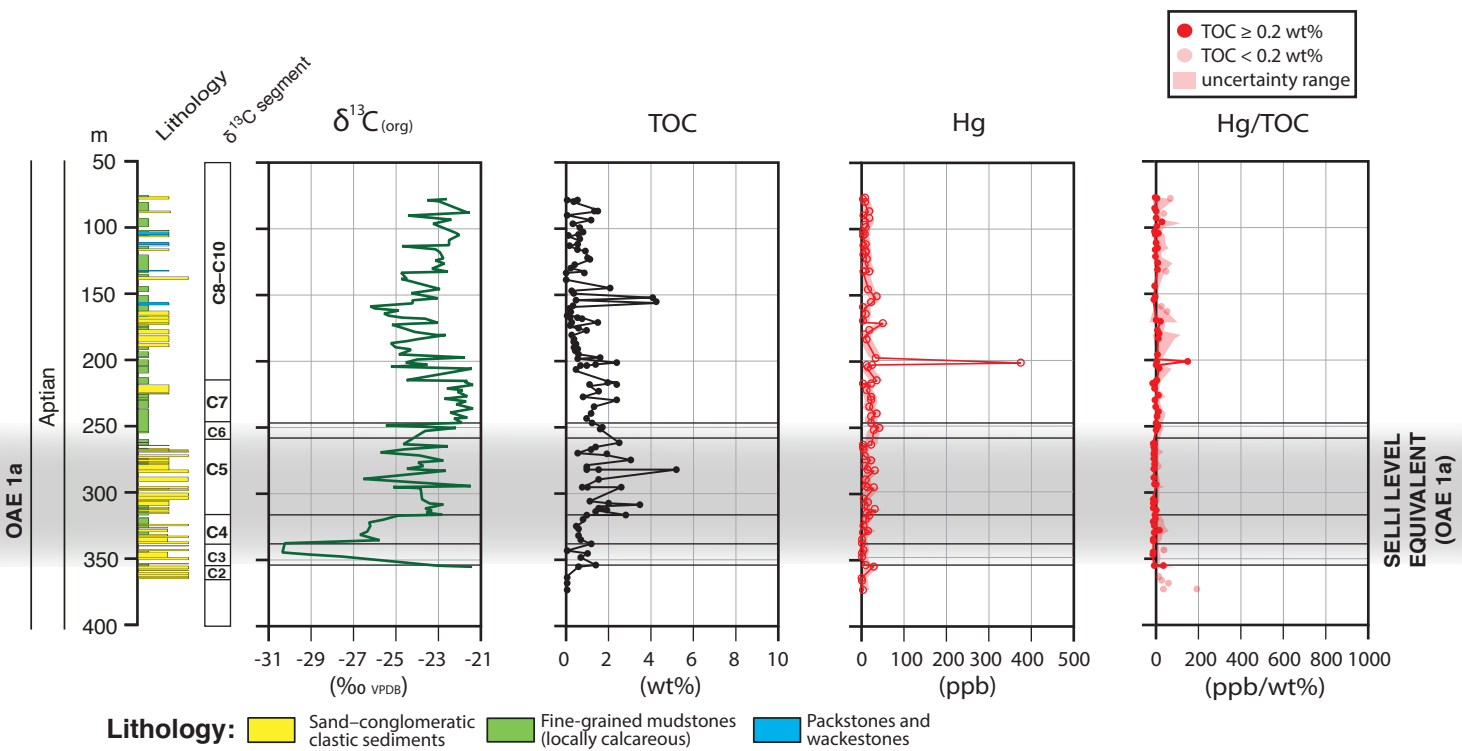


Figure 5

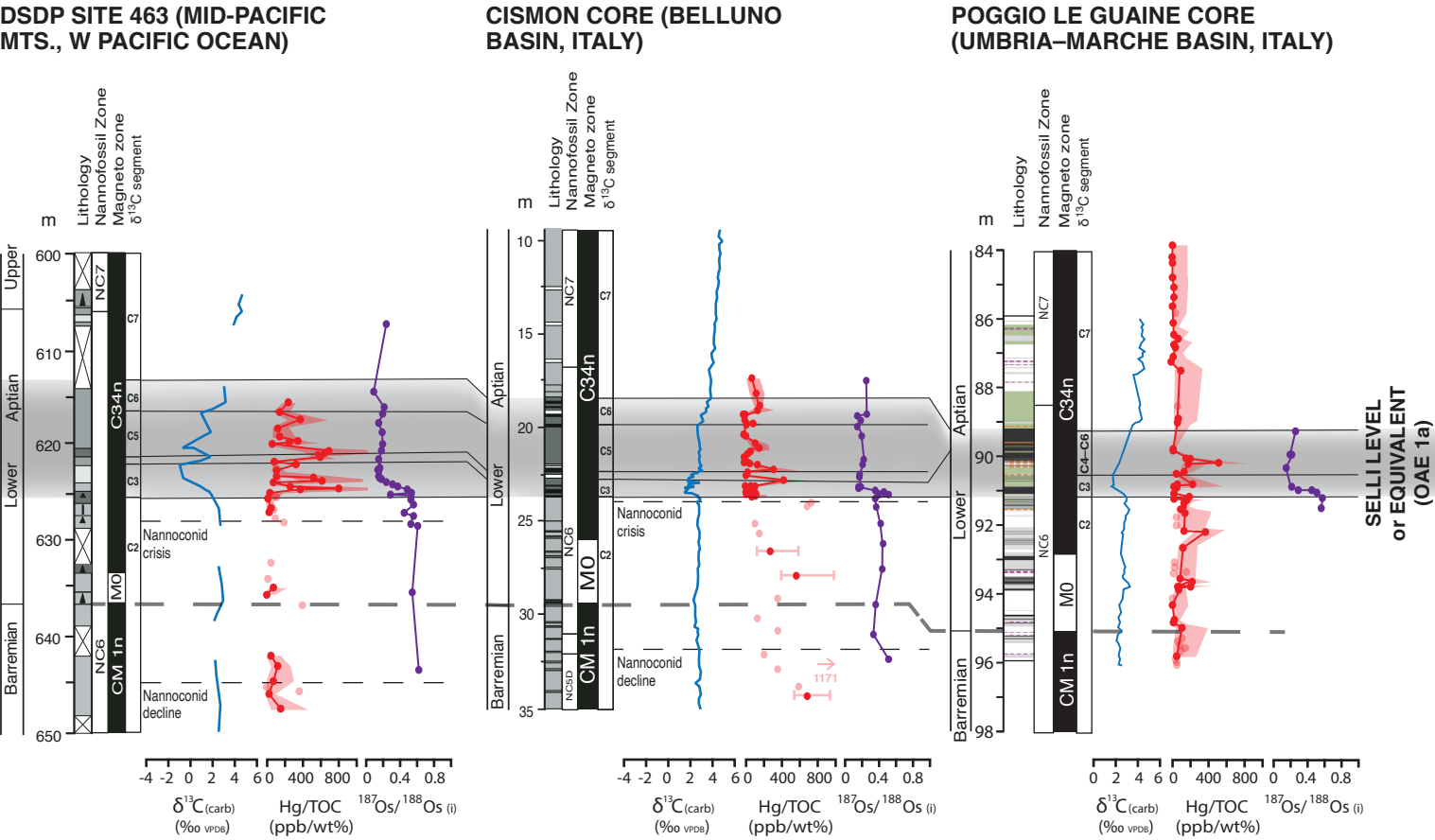


Figure 6

DSDP SITE 463 (MID-PACIFIC MOUNTAINS, W PACIFIC OCEAN)

